GaAs, AlAs, and $Al_xGa_{1-x}As$: Material parameters for use in research and device applications

Sadao Adachi

Citation: Journal of Applied Physics **58**, R1 (1985); doi: 10.1063/1.336070
View online: https://doi.org/10.1063/1.336070
View Table of Contents: http://aip.scitation.org/toc/jap/58/3
Published by the American Institute of Physics

GaAs, AlAs, and $Al_xGa_{1-x}As$: Material parameters for use in research and device applications

Sadao Adachi[a)]
Musashino Electrical Communication Laboratory, Nippon Telegraph and Telephone Corporation, Musashino-shi, Tokyo 180, Japan

(Received 7 September 1984; accepted for publication 1 April 1985)

The $Al_xGa_{1-x}As$/GaAs heterostructure system is potentially useful material for high-speed digital, high-frequency microwave, and electro-optic device applications. Even though the basic $Al_xGa_{1-x}As$/GaAs heterostructure concepts are understood at this time, some practical device parameters in this system have been hampered by a lack of definite knowledge of many material parameters. Recently, Blakemore has presented numerical and graphical information about many of the physical and electronic properties of GaAs [J. S. Blakemore, J. Appl. Phys. **53**, R123 (1982)]. The purpose of this review is (i) to obtain and clarify all the various material parameters of $Al_xGa_{1-x}As$ alloy from a systematic point of view, and (ii) to present key properties of the material parameters for a variety of research works and device applications. A complete set of material parameters are considered in this review for GaAs, AlAs, and $Al_xGa_{1-x}As$ alloys. The model used is based on an interpolation scheme and, therefore, necessitates known values of the parameters for the related binaries (GaAs and AlAs). The material parameters and properties considered in the present review can be classified into sixteen groups: (1) lattice constant and crystal density, (2) melting point, (3) thermal expansion coefficient, (4) lattice dynamic properties, (5) lattice thermal properties, (6) electronic-band structure, (7) external perturbation effects on the band-gap energy, (8) effective mass, (9) deformation potential, (10) static and high-frequency dielectric constants, (11) magnetic susceptibility, (12) piezoelectric constant, (13) Fröhlich coupling parameter, (14) electron transport properties, (15) optical properties, and (16) photoelastic properties. Of particular interest is the deviation of material parameters from linearity with respect to the AlAs mole fraction x. Some material parameters, such as lattice constant, crystal density, thermal expansion coefficient, dielectric constant, and elastic constant, obey Vegard's rule well. Other parameters, e.g., electronic-band energy, lattice vibration (phonon) energy, Debye temperature, and impurity ionization energy, exhibit quadratic dependence upon the AlAs mole fraction. However, some kinds of the material parameters, e.g., lattice thermal conductivity, exhibit very strong nonlinearity with respect to x, which arises from the effects of alloy disorder. It is found that the present model provides generally acceptable parameters in good agreement with the existing experimental data. A detailed discussion is also given of the acceptability of such interpolated parameters from an aspect of solid-state physics. Key properties of the material parameters for use in research work and a variety of $Al_xGa_{1-x}As$/GaAs device applications are also discussed in detail.

TABLE OF CONTENTS

I. INTRODUCTION

The alloy system $Al_xGa_{1-x}As$/GaAs is potentially of great importance for many high-speed electronics and optoelectronic devices, because the lattice parameter difference between GaAs and $Al_xGa_{1-x}As$ ($0 \leqslant x \leqslant 1.0$) is very small

a) Present address: Atsugi Electrical Communication Laboratory, Nippon Telegraph and Telephone Corporation, Atsugi-shi, Kanagawa 243-01, Japan.

 0021-8979/85/1500R1-29$02.40

(less than 0.15% at 300 K), which promises an insignificant concentration of undesirable interface states. The band-gap energy in $Al_xGa_{1-x}As$, and its dependence on the alloy composition are known to be one of the most important device parameters, and has received considerable attention in the past. However, unfortunately, transport- and optoelectronic-device parameters in this system have been hampered to date by a lack of definite knowledge of many basic material parameters. This necessitates the use of some sort of an interpolation scheme. An interpolation scheme is essentially based on known values of the physical constants for the related end compounds (binaries). Although any interpolation scheme is still open to experimental verification, it provides more useful and reliable material parameters over the entire range of alloy composition. However, some kinds of material parameters, e.g., lattice thermal conductivity (see Sec. III E), exhibit strong nonlinearity or discontinuity with respect to alloy composition. In such a case, attention must be carefully paid to the interpolated values. Recently, Adachi[1-6] and Olsen *et al.*[7] have obtained several material parameters of $In_{1-x}Ga_xAs_yP_{1-y}$ quaternaries from the interpolation scheme, and found a good agreement with the existing experimental data. However, little has been reported on the subject for the $Al_xGa_{1-x}As$ ternary. This is a motivation of the present work.

The purpose of this paper is threefold: (i) to obtain various material parameters of $Al_xGa_{1-x}As$ alloy based on the interpolation scheme, (ii) to discuss the acceptability of such interpolated parameters from an aspect of solid-state physics, and (iii) to present key properties of the material parameters for a variety of fundamental research and device applications. In Sec. II, a theoretical model used in this study is described. This model is based on an interpolation scheme, and the effects of compositional variations are properly taken into account in the model. In Secs. III–V, we present and discuss various material parameters of $Al_xGa_{1-x}As$ alloy. The parameters derived are also used with wide success to make clear general properties of this alloy. Of particular interest is the deviation of material parameters from linearity with respect to AlAs mole fraction x. Detailed discussion is given from this point of view. Finally, in Sec. VI, the conclusions obtained in the present study are summarized briefly.

II. THEORETICAL BASIS

An interpolation scheme is known to be a useful tool for estimating some physical parameters of alloy compounds.[1-8] If one uses linear interpolation, the ternary material parameter (T) can be derived from binary parameters (B's) by

$$T_{A_xB_{1-x}C}(x) = xB_{AC} + (1-x)B_{BC} \equiv a + bx, \tag{1}$$

for alloys of the form given by $A_xB_{1-x}C$, where $a \equiv B_{BC}$ and $b \equiv B_{AC} - B_{BC}$. Some material parameters, however, deviate largely from the linear relation of Eq. (1), and have an approximately quadratic dependence on the mole fraction of one compound x. The ternary material parameter, in such a case, can be very efficiently approximated by the relationship:

$$T_{A_xB_{1-x}C}(x) = xB_{AC} + (1-x)B_{BC} + C_{A\text{-}B}x(1-x) \equiv a + bx + cx^2, \tag{2}$$

where $a \equiv B_{BC}$, $b \equiv (B_{AC} - B_{BC} + C_{A\text{-}B})$, and $c \equiv -C_{A\text{-}B}$. $C_{A\text{-}B}$ is a contribution arising from the lattice disorder generated in the ternary system $A_xB_{1-x}C$ by the distribution of A and B atoms in one of the two sublattice sites. The parameter $c(C_{A\text{-}B})$ is usually called a "bowing" or "nonlinear" parameter.

It is well known from the literature[9] that the critical-point energy is a typical case exhibiting nonlinear dependence of the value on alloy composition. Let us now consider, as an example, the problem of the electronic-band structure of semiconductor alloy systems. Van Vechten and Bergstresser[9] developed a physical model for the calculation of c based on the Phillips's dielectric theory of electronegativity.[10] The deviation from linearity is considered to be due to two terms involving c_i, the intrinsic bowing parameter due to the virtual crystal approximation, and c_e, and the extrinsic bowing parameter due to aperiodicity in the alloy lattice;

$$c = c_i + c_e. \tag{3}$$

The values of c_i for many of the III-V ternary alloys are given by Van Vechten and Bergstresser.[9] The extrinsic term c_e is taken to be proportional to C_{AB}^2, i.e., to the square of the electronegativity difference between the atoms A and B for the alloy $A_xB_{1-x}C$;

$$c_e = C_{AB}^2/A', \tag{4}$$

where A' is the proportionality factor. Figure 1 shows the experimental values of c versus the electronegativity difference (END) between the same-group atoms (in parenthesis) for some of the interesting III-V ternary alloys. The parameters c considered here correspond to those of the lowest

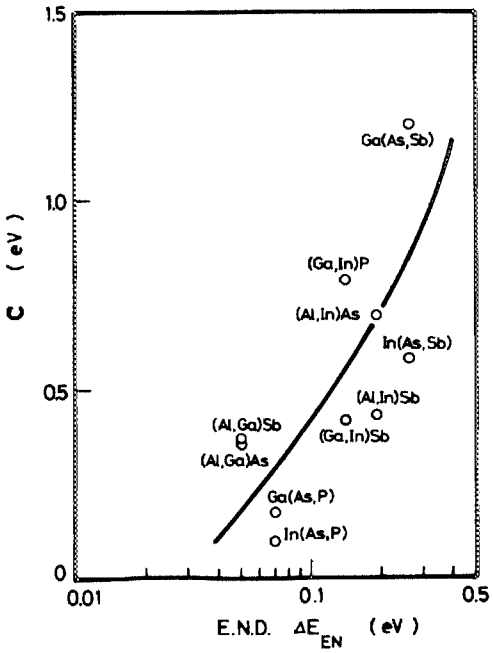

FIG. 1. Experimental values of the lowest-direct-gap bowing parameter c vs the electronegativity difference ΔE_{EN} between the same-group atoms (in parenthesis) for a number of the interesting III-V ternary alloys.

direct band gaps $E_0(\Gamma_8^v - \Gamma_6^c)$, and are gathered from many sources. The electronegativity values for the atoms are taken from a tabulation of Ref. 11. One can easily understand from this figure that the bowing parameter c of the electronic-band energy depends on the electronegativity difference between the same-group atoms in the III-V ternary alloys. Some kinds of the material parameters, e.g., lattice thermal conductivity (see Sec. III E), also exhibit very strong nonlinearity with respect to the alloy composition which, in this case, arises from the point-defect scattering due to the atomic weight difference and its constituents. In the following, we obtain various physical parameters of $Al_xGa_{1-x}As$ alloy by using the interpolation scheme and discuss the acceptability of such parameters from an aspect of the solid-state physics.

III. MECHANICAL AND THERMAL PROPERTIES

A. Lattice constant and crystal density

Some of the III-V compounds, and in particular GaAs and AlAs, form crystals with the zinc-blende arrangement. The zinc-blende structure is based on the cubic space group $F\bar{4}3m$. There are four molecules in a unit cell. Because of the small lattice parameter distance between GaAs and AlAs (see Table I), their ternary solutions are the closest in the III-V systems to being ideal and the alloys are among the easiest to prepare by epitaxial growth.[12] It is well known that the lattice constant a obeys Vegard's law in many of the III-V ternary alloys. For this reason we show in Fig. 2 the linear variation of the lattice constant with x for $Al_xGa_{1-x}As$ ter-

TABLE I. Bulk material parameters for GaAs, AlAs, and $Al_xGa_{1-x}As$. Validity of the material parameters for $Al_xGa_{1-x}As$ ternary is described in detail in the text.

Parameter	GaAs	AlAs	$Al_xGa_{1-x}As$
Space group	$F\bar{4}3m$[a]	$F\bar{4}3m$[a]	$F\bar{4}3m$
Lattice constant a (Å)	5.6533[b]	5.6611[c]	$5.6533 + 0.0078x$
Crystal density g (g/cm^3)	5.360[d]	3.760[e]	$5.36 - 1.6x$
Melting point (°C)	1238[f]	1740[g]	$1238 - 58x + 560x^2$[t] $1238 + 1082x - 560x^2$[u]
Thermal expansion coefficient α_{th} ($\times 10^{-6}$ °C)	6.4[h]	5.2[i]	$6.4 - 1.2x$
Elastic stiffness constant C_{ij} ($\times 10^{11}$ dyn/cm^2)			
C_{11}	11.88[j]	12.02[k]	$11.88 + 0.14x$
C_{12}	5.38[j]	5.70[k]	$5.38 + 0.32x$
C_{44}	5.94[j]	5.89[k]	$5.94 - 0.05x$
Elastic compliance constant S_{ij} ($\times 10^{-12}$ cm^2/dyn)			
S_{11}	1.17[j]	1.20[k]	$1.17 + 0.03x$
S_{12}	0.37[j]	0.39[k]	$0.37 + 0.02x$
S_{44}	1.68[j]	1.70[k]	$1.68 + 0.02x$
Young's modulus Y ($\times 10^{11}$ dyn/cm^2)	8.53[l]	8.35[l]	$8.53 - 0.18x$
Poisson's ratio P	0.31[l]	0.32[l]	$0.31 + 0.1x$
Bulk modulus B ($\times 10^{11}$ dyn/cm^2)	7.55[l]	7.81[l]	$7.55 + 0.26x$
Anisotropy factor A	0.55[l]	0.54[l]	$0.55 - 0.01x$
Compressibility C ($\times 10^{-12}$ dyn/cm^2)	1.33[l]	1.28[l]	$1.33 - 0.05x$
LO-phonon energy $\hbar\omega_{LO}$ (meV)			
GaAs-type	36.25[m]	...	$36.25 - 6.55x + 1.79x^2$
AlAs-type	...	50.09[m]	$44.63 + 8.78x - 3.32x^2$
TO-phonon energy $\hbar\omega_{LO}$ (meV)			
GaAs-type	33.29[m]	...	$33.29 - 0.64x - 1.16x^2$
AlAs-type	...	44.88[m]	$44.63 + 0.55x - 0.30x^2$
Specific heat C_P (cal/g deg)	0.08[n]	0.11[o]	$0.08 + 0.03x$
Debye temperature θ_D (K)	370[p]	446[q]	$370 + 54x + 22x^2$
Lattice thermal resistivity W (deg cm/W)	2.27[r]	1.10[s]	$2.27 + 28.83x - 30x^2$

[a] The principal structure type for GaAs and AlAs is cubic zinc-blende, in which the atoms are tetrahedrally bound in network arrangements related to those of the group IV semiconductors.

[b] C. M. H. Driscoll, A. F. W. Willoughby, J. B. Mullin, and B. W. Straughan, *Gallium Arsenide and Related Compounds* (Inst. of Physics, London, 1975), p. 275.

[c] J. Whitaker, Solid-State Electron. **8**, 649 (1965).

[d] Calculated as described in the text. L. R. Weisberg and J. Blanc [J. Appl. Phys. **34**, 1002 (1963)] give $g = 5.316$ g/cm^3.

[e] Calculated as described in the text. J. D. Wiley [*Semiconductors and Semimetals* (Academic, New York, 1975), Vol. 10, p. 91] gives $g = 3.598$ g/cm^3.

[f] M. B. Panish, J. Crystal Growth **27**, 6 (1974).

[g] H. Kressel and H. Nelson, *Physics of Thin Films* (Academic, New York, 1973), Vol. 7, p. 115.

[h] M. E. Straumanis, J.-P. Krumme, and M. Rubenstein, J. Electrochem. Soc. **114**, 640 (1967).

[i] M. Ettenberg and R. J. Paff, J. Appl. Phys. **41**, 3926 (1970).

[j] T. B. Bateman, H. J. McSkimin, and J. M. Whelan, J. Appl. Phys. **30**, 544 (1959).

[k] Estimated in the present study (see text).

[l] Calculated from the stiffness and compliance constants.

[m] These are the long-wavelength, optical-phonon energies taken from O. K. Kim and W. G. Spitzer [J. Appl. Phys. **50**, 4362 (1979)].

[n] Y. S. Toulouskian, R. K. Kirby, R. E. Taylor, and T. Y. R. Lee, Thermophys. Prop. Matter **13**, 747 (1977).

[o] U. Piesbergen, *Semiconductors and Semimetals* (Academic, New York, 1966), Vol. 2, p. 49.

[p] U. Piesbergen, Z. Naturforsch. Teil. A **18**, 141 (1963).

[q] Calculated as described in the text.

[r] P. D. Maycock, Solid-State Electron. **10**, 161 (1967).

[s] M. A. Afromowitz, J. Appl. Phys. **44**, 1292 (1973).

[t] This gives the solidus-surface curve [M. B. Panish and M. Ilegems, *Progress in Solid State Chemistry* (Pergamon, Oxford, 1972), Vol. 7, p. 39].

[u] This gives the liquidus-surface curve [M. B. Panish and M. Ilegems, *Progress in Solid State Chemistry* (Pergamon, Oxford, 1972), Vol. 7, p. 39].

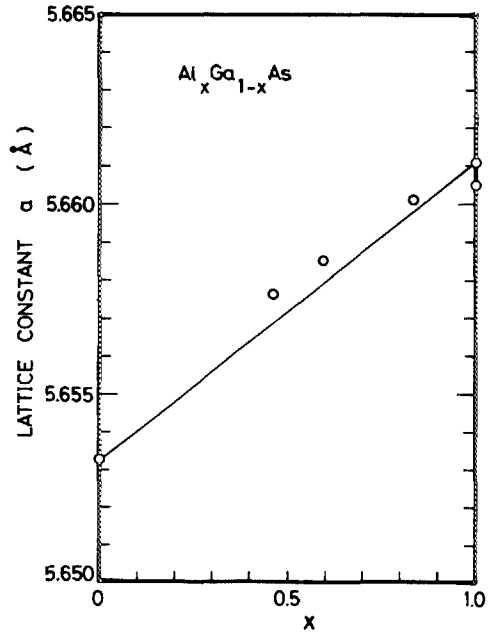

FIG. 2. Variation of the lattice constant a for $Al_xGa_{1-x}As$ ternary as a function of composition x. The data points are taken from GaAs from Ref. 13, for AlAs from Refs. 14 and 15, and for $Al_xGa_{1-x}As$ from Ref. 16.

nary. Measurements of a for AlAs have yielded slightly different values ranging from 5.6605 to 5.6611 Å. The data points shown in the figure are taken for GaAs from Ref. 13, for AlAs from Ref. 14 (5.6605 Å) and from Ref. 15 (5.6611 Å). Also included in Fig. 2 are the results of Rowland and Smith's measurements[16] made on $Al_xGa_{1-x}As$ epitaxial layers. Their data are thought to correspond to the expected values given by Vegard's law.

The crystal density g is one of the simplest and important material parameters. If an accurate lattice constant is available, the calculation of g gives in principle a good reliable value. Our calculated value of g for GaAs is, in fact, in good agreement with the experimental data.[17] Various III-V binaries, except AlAs, also showed a good agreement between the experiments and calculated values. (It was found that the differences between the calculated and experimental values are 0.83% for GaAs, 0.77% for CaP, 0.81% for InAs, 0.88% for InP, and 0.67% for AlSb). The data of Wiley for AlAs ($g = 3.598$ g/cm^3),[18] however, differs significantly from the calculated value ($g = 3.760$ g/cm^3). This gives an error of 4.5%. Therefore, at this time we are not considering his data. The calculated value of g for $Al_xGa_{1-x}As$ alloy, as a function of x, is an almost linear relationship given by

$$g(x) = 5.36 - 1.6x. \tag{5}$$

B. Melting point

Phase diagrams in crystal growth serve primarily as a guide to the solution compositions which will yield the desired solid layer, although they are also necessary for the interpretation of growth kinetic data. We obtain from the phase diagrams of Refs. 12, 19, and 20 the surfaces of the Al-Ga-As system ($Al_xGa_{1-x}As$) as a function of x with a relatively good approximation as (in °C):

$$T_s = 1238 - 58x + 560x^2 \tag{6a}$$

for the solidus surface, and

$$T_l = 1238 + 1082x - 580x^2 \tag{6b}$$

for the liquidus surface. The phase diagram of this and other systems of interest is supported by experimental and theoretical studies (see, for example, Refs. 12 and 20).

C. Thermal expansion coefficient

The efficiency and performance of electron and optoelectronic devices could depend on the point and extended defects present in the material and how likely those defects are to be mobile under device operating conditions. In the case of ternaries, the expansion coefficient varies quite linearly with compositional variation as seen in Ref. 21 for $In_{1-x}Ga_xP$. We also found that the coefficients estimated from the linear interpolation scheme are in good agreement with the experimental data for $In_{1-x}Ga_xAs_yP_{1-y}$ quaternaries.[2] Thus, one can suppose that the linear interpolation scheme, Eq. (1), may provide reliable thermal expansion coefficients of $Al_xGa_{1-x}As$ ternaries. In fact, the film strain generated in $Al_xGa_{1-x}As$/GaAs heterostructure increases linearly with x as expected from the expansion coefficient difference obeying Vegard's rule (see Sec. IV D).

D. Lattice dynamic properties

The purpose of this subsection is to examine the lattice dynamic properties of the alloy system $Al_xGa_{1-x}As$ by seeking generalizations which can be useful in estimating the properties of the alloy.

The crystals GaAs, AlAs, and $Al_xGa_{1-x}As$ alloy crystallize in the zinc-blende type structure, and so the elastic stiffness tensor $\mathbf{C}$ takes the form:[22]

$$\mathbf{C} = \begin{bmatrix} C_{11} & C_{12} & C_{12} & 0 & 0 & 0 \\ C_{12} & C_{11} & C_{12} & 0 & 0 & 0 \\ C_{12} & C_{12} & C_{11} & 0 & 0 & 0 \\ 0 & 0 & 0 & C_{44} & 0 & 0 \\ 0 & 0 & 0 & 0 & C_{44} & 0 \\ 0 & 0 & 0 & 0 & 0 & C_{44} \end{bmatrix}. \tag{7}$$

To our knowledge, there is no experimental data on the elastic stiffness constants C_{ij} of AlAs. This necessitates the use of some sort of means to estimate the unknown constants of this material. Keyes[23] found that the elastic constants of some group IV, III-V, and II-VI semiconductors are functions of their lattice constants only. He defined from a dimensional analysis an elastic constant $C_0 = e^2/b^4$, where e is the electronic charge and b is the distance between nearest-neighbor atoms. The elastic constants, reduced by the quantity C_0, have nearly the same value for the III-V binary compounds. This fact may be used to obtain the unknown elastic constants of other materials. Wiley,[18] indeed, estimated from this empirical relation the elastic constants of AlAs to be $C_{11} = 12.5$, $C_{12} = 5.34$, and $C_{44} = 5.42 \times 10^{11}$ dyn/cm^2.

We find here a simple relation between the elastic constants of various III-V compounds and their lattice constants. Figures 3–5 give, respectively, the plots of the values

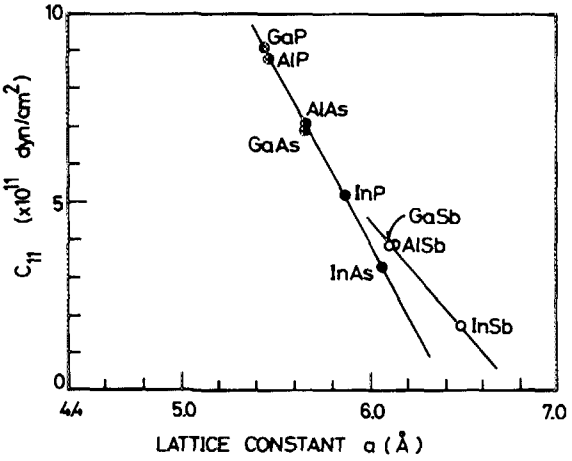

FIG. 3. Plots of the elastic constant C_{11} vs lattice constant a for some of the III-V binaries.

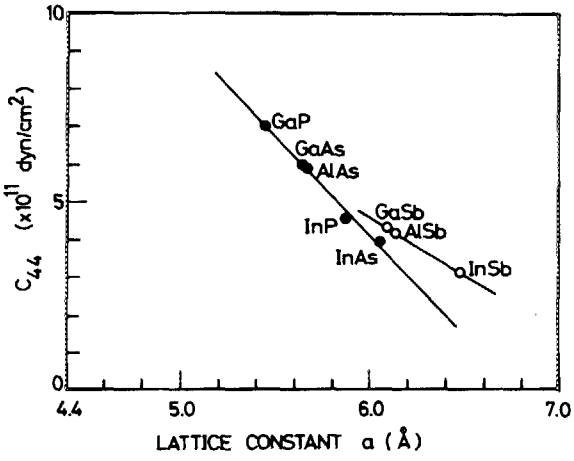

FIG. 5. Plots of the elastic constant C_{44} vs lattice constant a for some of the III-V binaries.

of C_{11}, C_{12}, and C_{44} versus the lattice constants for a number of the III-V binary compounds. The experimental data quoted here are gathered from many sources. The solid lines in the figures are the results of the least-square fit with the equation

$$C_{ij} = A_{ij}a + B_{ij}, \tag{8}$$

where A_{ij} and B_{ij} are the fitting parameters (constants) and a is the lattice parameter (in Å). The quantity C_{ij} of group III-V compounds, having the same crystal stucture, results in curves fitting well with Eq. (8). One can find that in Figs. 3–5 the solid lines are the curves on which the III-V compounds are expected to be found if the behavior can be generalized. As seen in the figures, the III-V compound materials can be classified into two groups [i.e., As(P)-based and Sb-based compounds]. The elastic properties can contribute to the long-range Coulomb forces in solids. Since As(P) and Sb form the outermost filled $4s(3s)$ and $5s$ and partially filled $4p(3p)$ and $5p$ electrons, respectively, the difference of $C_{ij} - a$ relations between the As(P)- and Sb-based compounds would arise from these electron states. The best-fit parameters determined here are as follows: $A_{11} = -9.273$ and $B_{11} = 64.510$ for the As(P)-based compounds, and $A_{11} = -5.824$ and $B_{11} = 44.497$ for the Sb-based compounds (C_{11} in units of 10^{11} dyn/cm^2); $A_{12} = -2.323$ and $B_{12} = 18.855$ for the As(P)-based compounds, and $A_{12} = -1.986$ and $B_{12} = 16.346$ for the Sb-based compounds (C_{12} in units of 10^{11} dyn/cm^2); $A_{44} = -5.218$ and $B_{44} = 35.433$ for the As(P)-based compounds, and $A_{44} = -2.984$ and $B_{44} = 22.488$ for the Sb-based compounds (C_{44} in units of 10^{11} dyn/cm^2). From the above results, we can estimate the elastic constants of AlAs to be $C_{11} = 12.02$, $C_{12} = 5.670$, and $C_{44} = 5.89 \times 10^{11}$ dyn/cm^2. These values are almost the same as those estimated from the Keyes's model.[18]

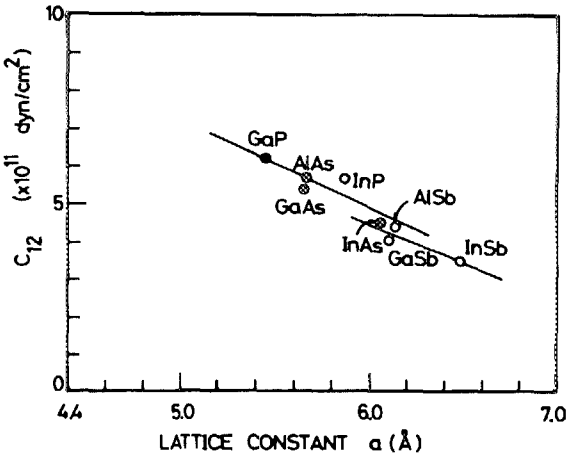

FIG. 4. Plots of the elastic constant C_{12} vs lattice constant a for some of the III-V binaries.

The elastic constants of the III-V binaries have been extensively measured, while to our knowledge there is no report up to date for the III-V ternaries or quaternaries. However, complete sets of the elastic constants have been obtained for relatively few single-crystal metallic alloys (Ag-Au, Au-Cd, Au-Zn, etc.).[24] The effect of variation of composition on the elastic properties of a nonmetallic substance has also been studied, e.g., by Rao,[25] who investigated the potassium-chromium alums over the complete range of composition. It was found that the stiffness moduli increased quite uniformly with compsition from chromium to potassium alum. It seems, thus, the elastic constant of III-V ternaries is linear with compositional proportion. Moreover, the lattice parameter a in many of the III-V compounds is known to obey well Vegard's rule, i.e., to vary linearly with composition. The generalized relation of Eq. (8), then, supports a lienar relationship between a and the lattice constant C_{ij}. The interpolation scheme of Eq. (1) may, therefore, provide reliable elastic parameters for the ternary system $Al_xGa_{1-x}As$. The stiffness constants, C_{11}, C_{12}, and C_{44}, and compliance constants, S_{11}, S_{12}, and S_{44}, as a function of composition x for $Al_xGa_{1-x}As$ alloy are listed in Table I. The macroscopic theory of the elastic properties of solids is described in detail in tensor notation by Nye.[22] The elastic compliance tensor **S**, which has the same form as Eq. (7), is connected reciprocally with the tensor **C** through Hooke's relation.[2] The stiffness and compliance constants for

$Al_xGa_{1-x}As$ vary very slowly with composition x.

Young's modulus Y is not isotropic in the cubic zinc-blende-type crystals. The variation, thus, depends on the direction of the crystal axes. The modulus Y for the direction of the cube axes $\langle 100 \rangle$ is given by

$$Y = 1/S_{11}. \tag{9}$$

Poisson's ratio P, in this case, is written as

$$P = -S_{12}/S_{11}. \tag{10}$$

The bulk modulus B and anisotropy factor A, for the zinc-blende-type crystals are, respectively, given by

$$B = (C_{11} + 2C_{12})/3 \tag{11}$$

and

$$A = (C_{11} - C_{12})/2C_{44}. \tag{12}$$

The compressibility C is also given by

$$C = [(C_{11} + 2C_{12})/3]^{-1}. \tag{13}$$

The calculated values of these moduli are also listed in Table I. It can be found that our calculated values compare well with those of Kushwara,[26] who calculated the elastic moduli based on a bond-bending force model.

If the density g and stiffness constant C_{ij} of solids are known, one can calculate the bulk sound velocity v from the general relation:

$$v = (C_{ij}/g)^{1/2}. \tag{14}$$

Figures 6 and 7 show the variation of the wave velocities in $Al_xGa_{1-x}As$ alloy propagating in the [100] and [110] directions, respectively. The data of g and C_{ij} are taken from Table I. v_{LA} corresponds to the longitudinal-wave mode velocity, v_{T1} the fast transverse-wave mode velocity, and v_{T2} corresponds to the slow transverse-wave mode velocity.

The surface-acoustic waves are modes of propagation of elastic energy along the free boundary of an infinite half space. The amplitude of their displacement undergoes an

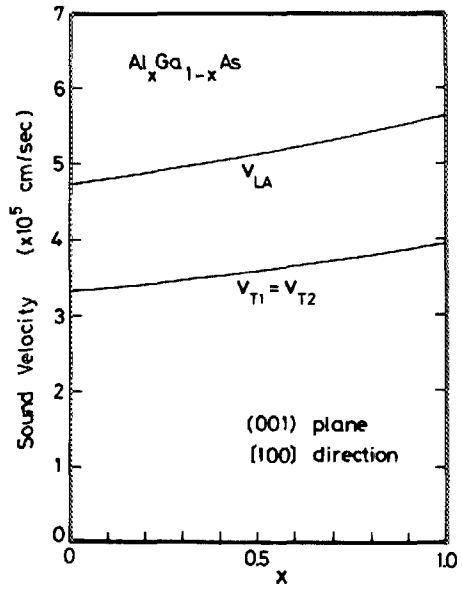

FIG. 6. Variation of the sound velocities propagating in the [100] direction in $Al_xGa_{1-x}As$ alloy.

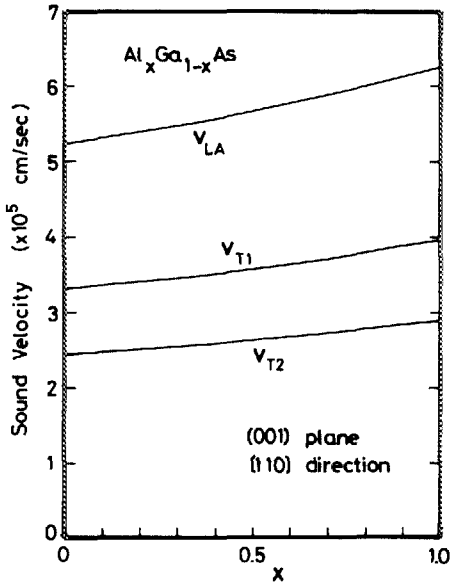

FIG. 7. Variation of the sound velocities propagating in the [110] direction in $Al_xGa_{1-x}As$ alloy.

exponential decay with depth below the free surface and vanishes within a distance of the order of two wavelengths.[27] The velocities of the surface waves v_{sw} in a zinc-blende type crystal are given by[28]

$$C_{11}\left(v_{sw}^2 - \frac{C_{44}}{g}\right)\left(v_{sw}^2 - \frac{C_{11}}{g} + \frac{C_{12}^2}{C_{11}g}\right)^2 = C_{44}v_{sw}^4\left(v_{sw}^2 - \frac{C_{11}}{g}\right), \tag{15a}$$

$$C_{11}\left(v_{sw}^2 - \frac{C_{44}}{g}\right)\left(v_{sw}^2 - \frac{2C_{44} + C_{12} + C_{11}}{2g} + \frac{C_{12}^2}{C_{11}g}\right)^2 = C_{44}v_{sw}^2\left(v_{sw}^2 - \frac{2C_{44} + C_{12} + C_{11}}{2g}\right). \tag{15b}$$

Equations (15a) and (15b) which are of third degree in v_{sw}^2 refer to the [100] and [110] propagation directions, respectively. They contain the three independent elastic constants of the crystal. Sapriel *et al.*[28] have recently performed experimental study (Brillouin and Raman scattering) on the acoustic properties of $Al_xGa_{1-x}As$ alloy and GaAs-$Al_xGa_{1-x}As$ superlattices. They have measured v_{sw} as a function of the Al -composition proportion for the $Al_xGa_{1-x}As$ alloy. Figures 8 and 9 show their experimental data (open circles) propagating in the [100] and [110] directions, respectively. The experimental data of Voltmer *et al.*[29] for GaAs is also shown in Fig. 9 by the vertical bar. The figures also compare the theoretical velocity variations versus x calcualted from Eq. (15) using a set of the elastic constants of ours [curve (1)] and of Keyes's model [curve (2)].[18] The experimental velocity variations versus x plotted in Figs. 8 and 9 could be approximated by the linear laws [curve (3)]: $v_{sw} = 2690 + 290x$ along [100] and $v_{sw} = 2817 + 315x$ along [110] (in units of 10^2 cm/s).[28] These curves join the experimental points well. However, there is a considerable disagreement between the theoretical curves [curves (1) and (2)] and experimental points. This is conspicuous at a region of larger x values. We have also calculated the velocity variation in the case where

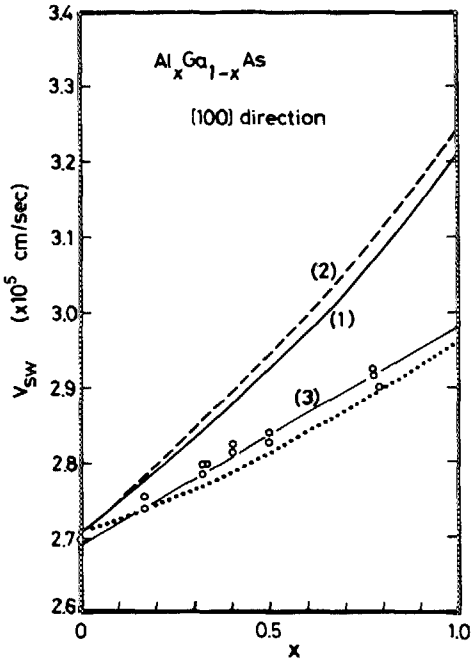

FIG. 8. Surface-acoustic-wave velocity vs composition x propagating in the [100] direction in $Al_xGa_{1-x}As$ alloy. The experimental data (open circles) are taken from Ref. 28. The curves (1) and (2) are calculated results using the set of lattice constants of ours and Keyes's model, respectively. The curve (3) joins the experimental points (see text). The dotted line is calculated from Appendix A.

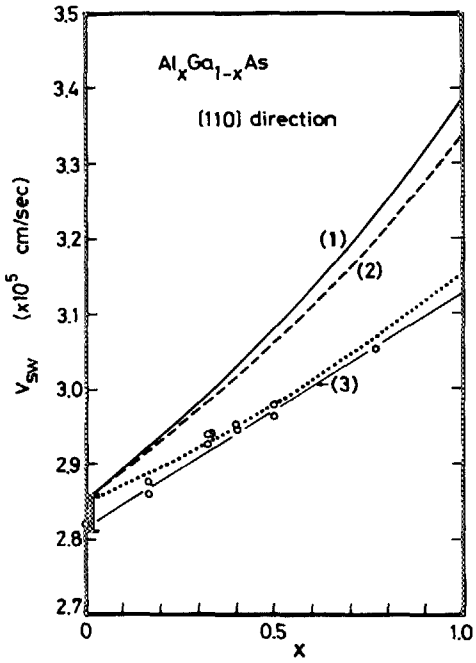

FIG. 9. Surface-acoustic-wave velocity vs composition x propagating in the [110] direction in $Al_xGa_{1-x}As$ alloy. The experimental data (open circles) are taken from Ref. 28. The data for GaAs (Ref. 29) is also shown by the vertical bar. The curves (1) and (2) are calculated results using the set of lattice constants of ours and Keyes's model, respectively. The curve (3) joins the experimental points (see text). The dotted line is calculated from Appendix A.

the elastic constants are kept constant versus x for $Al_xGa_{1-x}As$ as for GaAs and only the density variation is taken into account. The results obtained from this calculation are very similar to those of the curves (1) and (2). Sapriel *et al.*[28] have suggested that this probelm (i.e., disagreement) arises from a tendency of the elastic constants to *softening* which results from substitution of Ga by Al in the Ga sublattice. Introducing a reduced elastic constant, we can also obtain the compositional variation of v_{sw} which agrees well with the experimental data. We get from this consideration the lattice constants of AlAs to be $C_{11} \simeq 10.4$, $C_{12} \simeq 5.2$, and $C_{44} \simeq 5.2 \times 10^{11}$ dyn/cm^2 (see Appendix A). These values are considerably smaller than ours and those estimated by the Keyes's model. This problem is, thus, still open at the present time. Of course, it is interesting to make clear elastic-softening phenomena in alloy systems.

It is well known that the long-wavelength optical phonons in the III-V mixed crystal $A_xB_{1-x}C$ exhibit either a so-called one-mode or a two-mode behavior.[30] In the two-mode behavior, a longitudinal-transverse multiplet coinciding with that of the pure BC crystal when $x = 0$ evolves roughly linearly with the concentration of A towards the localized mode of a B atom in the AC crystal when $x = 1.0$, simultaneously the longitudinal-transverse splitting and intensity decrease to x. In the one-mode case, on the other hand, the multiplet of the pure BC crystal evolves towards the multiplet of the AC crystal. Some crystals exhibit both kinds of behavior in different concentration ranges. The optical phonons in the $Al_xGa_{1-x}As$ system exhibit the two-mode behavior through the whole compositional range, a property that has been studied in the past few years by many investigators.[31–34] The $Al_xGa_{1-x}As$ system, thus, has two couplets of the longitudinal optical (LO) and transverse optical (TO) modes; one is GaAs-like and the other is AlAs-like optical phonons. In the following, we derive numerical expressions of such GaAs-like and AlAs-like LO, TO phonon energies in the $Al_xGa_{1-x}As$ system. Effective LO and TO phonon energies in this system are also defined for convenience in use of these parameters. These phonon energies will be used to analyze various material properties in the following subsections (see, for example, Secs. V D and V E).

There are many theoretical approaches to understand the long-wavelength, optical phonon properties in the alloy systems.[35–40] Kim and Spitzer[33] have provided confirmation of the two-mode behavior in the $Al_xGa_{1-x}As$ system and also reported additional Raman structures for the acoustic vibrations. The behavior has been well interpreted in terms of a modified random-element-isodisplacement model.[36] The experimental results of Kim and Spitzer are presented in Fig. 10. It is clear that the experimental points show nonlinear variation with composition x. The solid lines in the figure are the results of interpolation scheme of Eq. (2). A comparison with the experimental data shows a quite good agreement. The nonlinear parameters determined are as follows (in meV): $c = 1.79$ (GaAs-like) and -3.32 (AlAs-like) for the LO phonon energies, and $c = -1.16$ (GaAs-like) and -0.30 (AlAs-like) for the TO phonon energies. The LO and TO phonons play an important role in the study of optical and transport properties in solids. With the present result, one can easily use the LO and TO phonon energies in the

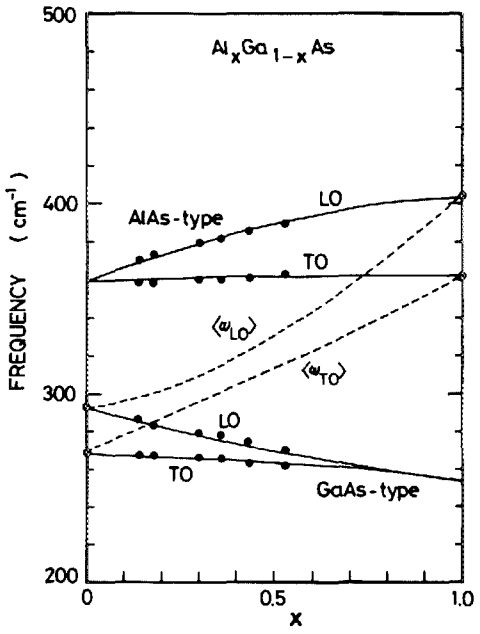

FIG. 10. Optical phonon energy as a function of composition x for $Al_xGa_{1-x}As$ alloy. The experimental data (solid circles) are taken from Ref. 33. The solid lines are interpolated results of Eq. (2). The compositional dependence of the effective phonon energies, $\langle\omega_{LO}\rangle$ and $\langle\omega_{TO}\rangle$, is shown by the dashed lines (see text).

$Al_xGa_{1-x}As$ system with optional Al(x) contents.

The exact theory of the electron-phonon interactions in alloys where there are two-mode phonons present has not been reported previously. In this case, it would be useful to define the effective phonon energy $\langle\omega_{LO(TO)}\rangle$ by the equation:

$$\langle\omega_{LO(TO)}\rangle(x) = (1-x)\omega^{G}_{LO(TO)}(x) + x\omega^{A}_{LO(TO)}(x), \quad (16)$$

where $\omega^{G}_{LO(TO)}(x)$ and $\omega^{A}_{LO(TO)}(x)$, respectively, are functions of the LO(TO) phonons for the GaAs-like and AlAs-like modes in the $Al_xGa_{1-x}As$ crystal. The effective phonon energies can, then, be numerically represented by (in meV)

$$\langle\omega_{LO}\rangle(x) = 36.25 + 1.83x + 17.12x^2 - 5.11x^3, \quad (17)$$

$$\langle\omega_{TO}\rangle(x) = 33.29 + 10.70x + 0.03x^2 + 0.86x^3. \quad (18)$$

The calculated results of these effective phonon energies as a function of x are also plotted in Fig. 10 by the dashed lines.

E. Lattice thermal properties

Investigation of the thermal properties in solids is an old topic which arises in strong connection with the fundamental physical properties of the solids.[41] In this subsection, we shall try to discuss and estimate various thermally related material parameters (e.g., Debye temperature and thermal conductivity) in $Al_xGa_{1-x}As$ alloy.

A major step forward in our knowledge concerns the thermal energy content of a solid. This leads us to one of the most essential thermal parameters which is known as the heat capacity or specific heat of the solid. Very few measurements of the specific heat are available for the III-V compounds. Toulouskian *et al.*[42] have given specific heat values (C_p) for GaAs between 10 and 1000 K. The value C_p of AlAs at 300 K was calculated by Piesbergen[43] from a Debye temperature to be 0.108 cal/g deg. Since no details of this parameter has been reported to date for semiconductor alloys, we estimate C_p for $Al_xGa_{1-x}As$ alloy based on the linear interpolation scheme with the corresponding binary data (see Table I). As we will see next, the Debye temperature of $Al_xGa_{1-x}As$ alloy shows very weak nonlinearity with composition x. The specific heat C_p can be represented adequately by this characteristic temperature. Thus, it seems that at least for $Al_xGa_{1-x}As$ alloy the linear interpolation method would provide generally acceptable C_p values.

The Debye temperature θ_D is a useful parameter in solid-state problems because of its inherent relationship to lattice vibration. The parameter θ_D can be used in characterizing the excitation of phonons and to describe various thermal phonomena such as specific heat[43] and lattice thermal conductivity.[41] The Debye temperatures of many materials are known very precisely from low-temperature measurements of the specific heat. Some materials, like AlAs, have not been investigated as yet, especially those where it was not possible to prepare large pure crystals. Marcus and Kennedy[44] have investigated the relation between the elastic constant and Debye temperature θ_D at 0 K in the Debye approximation. Steigmeier[45] has shown, using the Marcus–Kennedy formula, that it would be possible to estimate unknown Debye temperatures using simple material parameters such as the atomic mass and lattice constants. This consideration is based on the observation of Keyes (see Sec. III D) (i.e., the elastic constants of IV, III-V, and II-VI elements and compounds depend only on functions of their corresponding lattice constants). The formula of Steigmeier can now be written as

$$\theta_D(0) = (4.19\times10^{-8}/\sqrt{a^3M})\sqrt{C_{11}/C_0}\,f(r_1,r_2), \quad (19)$$

where a is the lattice constant, M the mean mass, $r_1 = (C_{11}-C_{12})/C_{11}$, $r_2 = C_{44}/C_{11}$, C_0 the reduced elastic constant of Keyes,[23] and $f(r_1,r_2)$ is an angular average over the reciprocal sound velocities in k space. Based on this formula and from various material parameters determined previously, we can obtain the Debye temperature $\theta_D(0)$ of $Al_xGa_{1-x}As$ alloy. Figure 11 shows the calculated $\theta_D(0)$ values as a function of x for $Al_xGa_{1-x}As$ alloy. Piesbergen[43] has also reported the temperature variation of θ_D for a number of the III-V compounds (AlSb, GaAs, GaSb, etc.). The values of θ_D at 77 and 300 K as a function of x for $Al_xGa_{1-x}As$ alloy are also shown in Fig. 11. These curves where obtained from their lattice constants and by extrapolating Piesbergen's binary data over the entire range of composition x. The estimated θ_D values vary quadratically with composition x, but the correction due to the bowing parameter is found to be very small.

Knowledge of lattice thermal conductivity (or thermal resistivity) of semiconductors forms an important part in the design of power dissipating devices, such as diodes, transistors, and semiconductor lasers.[41] The thermal conductivity value is also necessary in calculating the figure of merit for thermoelectric devices (e.g., Peltier devices). The thermal conductivity properties have been studied intensively for many III-V compounds, including some of the ternary and

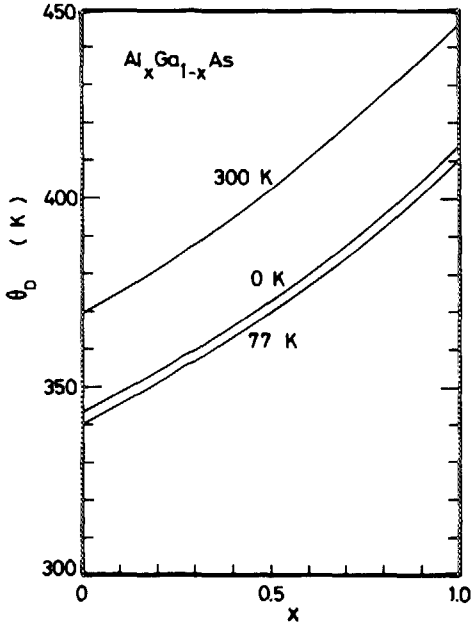

FIG. 11. Debye temperature θ_D as a function of composition x for $Al_xGa_{1-x}As$ alloy.

quaternary alloys. Reviews by Holland[41] and Maycock[46] thoroughly cover important theoretical and experimental aspects of the thermal conductivity properties of III-V compounds in detail and discuss the relevant literature. Semiconductor alloys are well suited for investigating the effects of imperfections on the lattice thermal conductivity. It is important to point out that when large numbers of foreign atoms are added to host lattice as in alloying, the thermal conductivity decreases significantly. An exact calculation of the lattice thermal conductivity is possible in principle, but lack of knowledge of various parameters (e.g., anharmonic forces and lattice vibration spectra) and the difficulty of obtaining exact solution of phonon-phonon interactions are formidable barriers to progress. It is, thus, interesting to investigate the consequence of a simple model which is more amenable to calculation.

Abeles[47] has proposed a phenomenological model to analyze the thermal conductivity of semiconductor alloys. The thermal conductivity has been expressed in terms of the lattice parameters and mean atomic weights of the alloy and its constituents. Agreement has been obtained between calculation and published experimental data on Ge-Si, GaAs-InAs, and InAs-InP alloys. Abele's model, however, requires various material parameters and adjustable constants to obtain the best fit between calculation and experiment. Because of this reason, a more simple and reliable model is thought to be needed in practical aspect.

A simple theoretical model has recently been proposed to analyze the compositional dependence of the thermal conductivity of semiconductor alloys.[3,48] This model is based on the interpolation scheme, namely Eq. (2). The model properly takes into account the concept of bowing factor as a term of ternary parameters and arises, in the case of the thermal conductivity, through strain and mass point defects. It has been found that the alloy disorder factor C_{A-B} in Eq. (2) can be characterized by the two alloyed elements A and B (i.e., by the mean atomic weights of A and B atoms) and not depend on the element C.[3] Figure 12 compared the calculated results of Eq. (2) to the experimental data of GaAs-AlAs alloy. The data are taken from Afromowitz.[49] The best-fit value of C_{Ga-Al} is found to be 30 W^{-1} deg cm. Agreement between the calculation and experimental data is excellent and represents the successful explanation of the compositional variation of the lattice thermal conductivity in the $Al_xGa_{1-x}As$ system. The thermal conductivity of $Al_xGa_{1-x}As/GaAs$ heterostructure laser devices can be calculated using a model of Joyce and Dixon[50] in which two-dimensional heat flow is assumed to proceed from an uniformly excited stripe to a constant-temperature heat sink on one face.

IV. BAND-STRUCTURE CONSEQUENCES

A. Electronic-band structure

There is a considerable theoretical and experimental interest in the electronic-band structure of GaAs, AlAs, and their mixed crystals for their various device applications.[51–63] There have been several determinations of the compositional dependence of the energy gaps (E_g's) in $Al_xGa_{1-x}As$.[57,61] Casey and Panish[61] suggested that the Γ direct gap ($\Gamma_8^v - \Gamma_6^c$) may be represented at 300 K by (in eV)

$$E_g^{\Gamma}(x) = 1.424 + 1.247x \quad (0 \leqslant x \leqslant 0.45), \tag{20a}$$

$$= 1.424 + 1.247x + 1.147(x - 0.45)^2, \ (0.45 < x \leqslant 1.0), \tag{20b}$$

while the X indirect ($\Gamma_8^v - X_6^c$) and L indirect ($\Gamma_8^v - L_6^c$), respectively, are taken as (in eV)

$$E_g^X(x) = 1.900 + 0.125x + 0.143x^2, \tag{21}$$

$$E_g^L(x) = 1.708 + 0.642x. \tag{22}$$

Lee *et al.*[57] also quoted the dependence of E_g's on x at room temperature in $Al_xGa_{1-x}As$ alloy as (in eV)

$$E_g^{\Gamma}(x) = 1.425 + 1.155x + 0.37x^2, \tag{23}$$

$$E_g^X(x) = 1.911 + 0.005x + 0.245x^2, \tag{24}$$

$$E_g^L(x) = 1.734 + 0.574x + 0.055x^2. \tag{25}$$

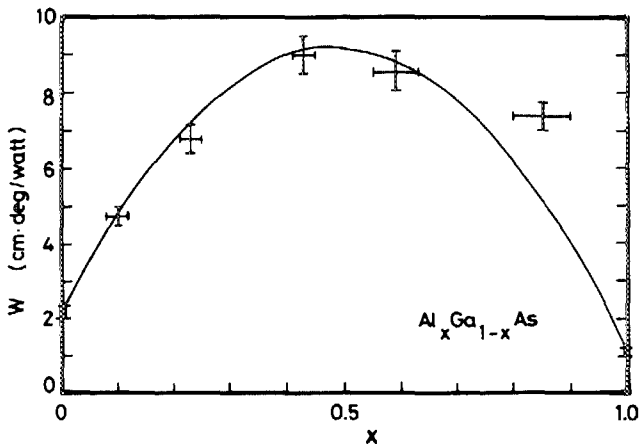

FIG. 12. Lattice thermal resistivity as a function of composition x for $Al_xGa_{1-x}As$ alloy. The solid line is a theoretical fit to the data (Ref. 49) using the present model [Eq. (2)].

These data indicate that the $\Gamma - X$ crossover occurs in the compositional range of $0.4 \lesssim x \lesssim 0.5$. This region of x where the bands cross is relatively uncertain at the present time.

As we will see later (Sec. V F and V G), optical properties of solids arise in strong connection with the critical-point energies of the solids. A series of critical-point energies can be obtained by using the interpolation scheme. Figure 13 shows a series of the calculated critical-point energies, E_0, $E_0 + \Delta_0$, E_1, $E_1 + \Delta_1$, E_0', $E_0' + \Delta_0'$, and E_2, versus x for $Al_xGa_{1-x}As$ alloy. The solid lines are the results of the linear interpolation scheme of Eq. (1). The binary data are taken for GaAs from Ref. 64 and for AlAs from Ref. 52 (see also Ref. 53). As already discussed in Sec. II, the interband transition energy of the III-V alloy system as a function of compositional variation is known to be nonlinear and can be generally described by a quadratic in the compositional parameter. This suggests that the system has a complex relation between the interband energy and compositional parameter through the effects of alloy disorder.

Stringfellow[59] has made theoretical estimates of the bowing parameters for various mixed III-V alloys based on the dielectric theory of electronegativity.[10] He obtained the calculated bowing parameters of $Al_xGa_{1-x}As$ alloy as $c_0 \simeq -0.03$ eV for the E_0 gap, $c_1 \simeq 0.0$ eV for the E_1 gap, and $c_2 \simeq 0.02$ eV for the E_2 gap. The only experimental results on various interband transitions in $Al_xGa_{1-x}As$ alloy are those of Berolo and Woolley,[54] who made electroreflectance measurements in the range 1–5 eV and obtained $c_0 = 0.26$ eV, $c_1 = 0.45$ eV, and $c_2 = 0.02$ eV. The dashed lines in Fig. 13 are given by Eq. (2) with the bowing parameters of Berolo and Woolley. The value of c_0 from Lee *et al.*[57] is 0.37 eV [see Eq. (23)]. The experimental data (Casey and Panish) shows a linear dependence of E_0 on x in the direct-gap range (i.e., $0 < x \leqslant 0.45$), but some bowing is necessary to have E_0 agree with experimental values at $0.45 < x \leqslant 1.0$ [see Eq. (20)]. There is no good agreement between the calculation (Stringfellow)[59] and experiment for c_0 and c_1, while those of c_2 show an excellent agreement. Electroreflectance measurements on AlAs have been carried out by Onton.[52] He obtained the spin-orbit splitting energy Δ_0 (0.275 eV). Parayanthal *et al.*[65] have also obtained the compositional dependence of Δ_0 for $(Al_xGa_{1-x})_{0.47}In_{0.53}As$ alloy by means of the electroreflectance experiment: $\Delta_0 = 0.37 + 0.10x - 0.10x^2$. By extrapolating this result, we obtain the value of Δ_0 for AlAs to be 0.3 eV. These experimental data agree well with the calculated value of Braunstein and Kane ($\Delta_0 = 0.29$ eV).[66] In Fig. 13, the linear interpolation scheme may provide slight reliable values especially for the $E_0(E_0 + \Delta_0)$-gap and the $E_1(E_1 + \Delta_1)$-gap energies.

The commonly used material parameters for constructing band diagrams for heterostructures involving two semiconductors are the electron affinities (χ_e's) and their difference, because χ_e is a material property that is invariant with normal doping.[67] The conduction-band edge of III-V compounds is well characterized by electron orbitals of the group III (cation) atoms. The variation of χ_e for some of the III-V binaries with respect to the corresponding group III (cation) atomic numbers is plotted in Fig. 14. The numerical values of χ_e are taken from a tabulation of Milnes and Feucht.[67] It is easily understood from the figure that there is an increase in χ_e with increase in the atomic number of the cation atom.

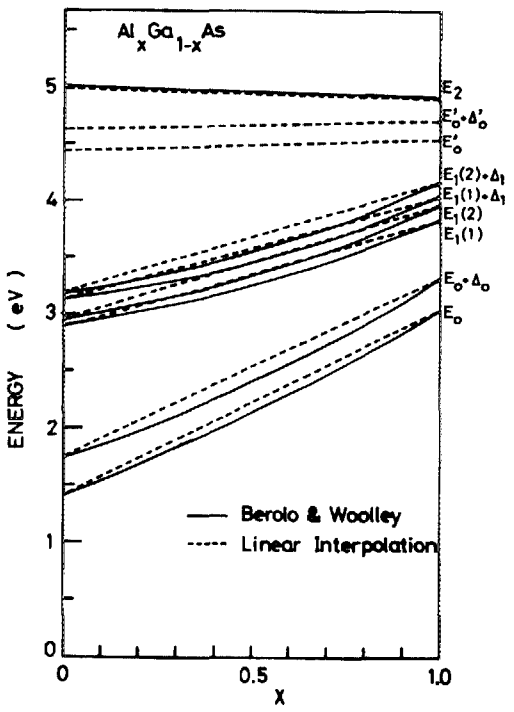

FIG. 13. A series of the critical-point energies as a function of composition x for $Al_xGa_{1-x}As$ alloy (see text).

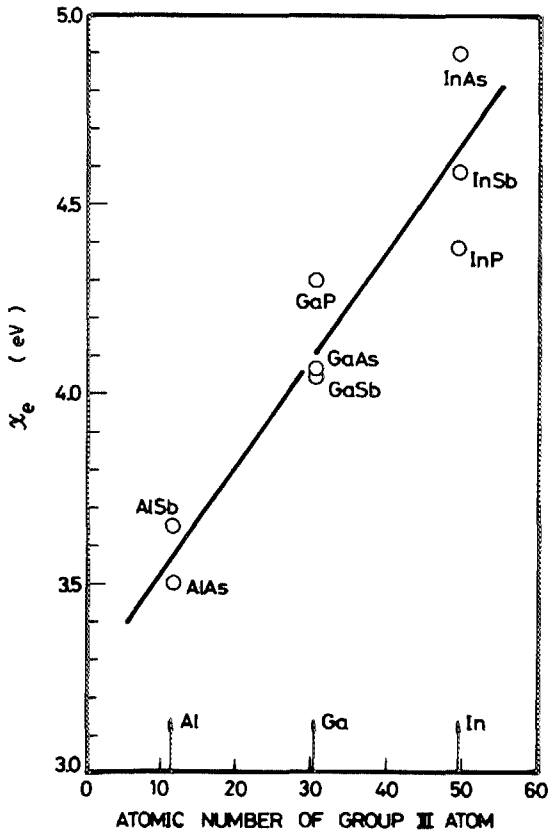

FIG. 14. Variation of the electron affinity χ_e for some of the III-V binaries vs the corresponding group-III (cation) atomic number.

From the binary data of χ_e[68–70] and compositional dependence of the band-gap energies, we can obtain the electron affinities of $Al_xGa_{1-x}As$ alloy as (in eV)

$$\chi_e(x) = 4.07 - 1.1x \tag{26a}$$

for $0 \leqslant x \leqslant 0.45$, and

$$\chi_e(x) = 3.64 - 0.14x \tag{26b}$$

for $0.45 < x \leqslant 1.0$. By the aid of Anderson's electron affinity rule,[71] we can also predict the conduction-band discontinuity ΔE_c (eV) between GaAs and $Al_xGa_{1-x}As$ layers[72,73]:

$$\Delta E_c(x) = 1.1x \tag{27a}$$

for $0 \leqslant x \leqslant 0.45$, and

$$\Delta E_c(x) = 0.43 + 0.14x \tag{27b}$$

for $0.45 < x \leqslant 1.0$.

B. External perturbation effects on the E_g-gap energy

Studies on group III-V compounds have established the general nature of the shift of the three conduction band minima Γ, X, and L with hydrostatic pressure.[74] The pressure variation of the band gap for GaAs (dE_g^{Γ}/dP), in particular, has been studied by different methods with reasonable agreement between them. Lifshitz *et al.*[75] have found empirical relation that in III-V semiconductors with the same anion the pressure coefficient varies inversely with the lowest direct gap. They obtained from this relation dE_g/dP for AlAs to be $\sim 1.0\times10^{-5}$ eV/bar. We now plot in Fig. 15 the numerical values of dE_g/dP as a function of Phillips's ionicity f_i for a number of the III-V binary compounds. The Phillips's ionicity is known to be one of the most essential parameters to characterize various properties of solids.[76] One can understand from this figure that there is a decrease in dE_g/dP with increasing f_i. We can then expect dE_g/dP for AlAs to be $\sim 1.3\times10^{-5}$ eV/bar and that for $Al_xGa_{1-x}As$ alloy to be a smoothly decreasing function of x [since f_i for $Al_xGa_{1-x}As$ should decrease smoothly from 0.310 for GaAs to 0.274 for AlAs (see Table II)]. Lifshitz *et al.*,[75] on the other hand, have found that the experimental pressure coefficient dE_g/dP for $Al_xGa_{1-x}As$ increases linearly up to $x = 0.25$ and then decreases nonlinearly. However, their data is limited to the compositional proportion of $0 \leqslant x \leqslant 0.5$. The nonlinear decrease in dE_g/dP seems to be due to the effects of the $\Gamma - X(L)$ crossover in this compositional range. Thus, there is uncertainty on the coefficient dE_g/dP for $Al_xGa_{1-x}As$, and it would be required a precise experimental data over the entire range of alloy composition. Numerical value for AlAs in Table II is extrapolated one of Ref. 75. The pressure coefficients of the E_g^X and E_g^L gaps are also listed in the table. In these cases, a lack of the values for AlAs hampered the use of the interpolation scheme. Therefore, we postulate that the values of AlAs are supposed to be the same as those of GaP.[77] This consideration is based on the following reasons. It has been reported that three types of the indirect transitions are present in GaP below the direct $\Gamma_8^v - \Gamma_6^c$ gap; $\Gamma_8^v - X_6^c$ transition near 2.25 eV (300 K),[78] $\Gamma_8^v - X_7^c$ transition near 2.48 eV (300 K),[79] and $\Gamma_8^v - L_6^c$ transition near 2.67 eV (78 K).[80] These band structure and energies are very similar to those of AlAs. The $X_6^c - L_6^c - \Gamma_6^c$ conduction-band ordering of GaP is also the same as that of AlAs.

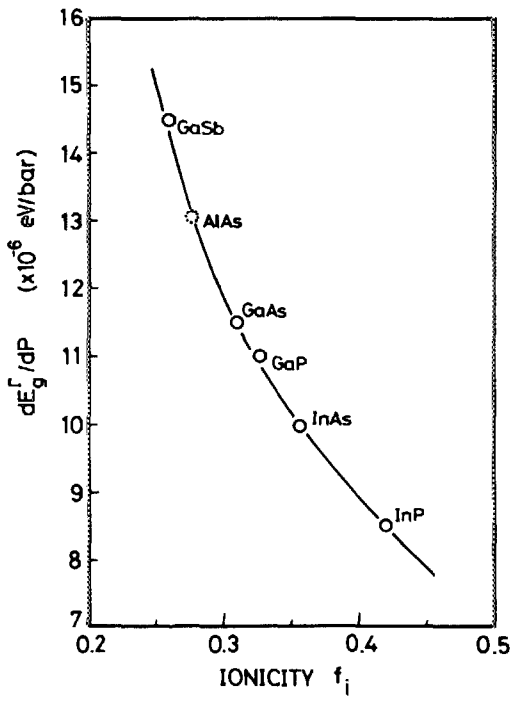

FIG. 15. Trends in dE_g^{Γ}/dP as a function of Phillips's ionicity f_i for some of the III-V binaries.

The temperature coefficient of the band gap (dE_g^{Γ}/dT) is known to be linear for temperatures higher than 150 K, as in most of the semiconductors. Zvara[81] has obtained the value of dE_g^{Γ}/dT for GaAs to be -3.95×10^{-4} eV/deg. Zucca and Shen[82] have determined the coefficients dE_1/dT and dE_2/dT of GaAs to be -5.3×10^{-4} and 13.6×10^{-4} eV/deg, respectively, from wavelength modulation spectroscopy. We now adopt these experimental data as the temperature variations of the indirect gaps of this material (i.e., we assumed that $dE_1/dT \simeq dE_g^L/dT$ and $dE_2/dT \simeq dE_g^X/dT$ since no detailed values of the temperature coefficients of such indirect-gap energies are available at the present time). Monemar[83] has measured the temperature variations of the fundamental-gap energies (E_g^{Γ} and E_g^X) for AlAs. The data obtained by him are as follows: $dE_g^{\Gamma}/dT = -5.1\times10^{-4}$ eV/deg and $dE_g^X/dT = -3.6\times10^{-4}$ eV/deg. It has been found that for $In_{1-x}Ga_xAs_yP_{1-y}$ quaternaries the linear interpolation method provides relatively good values of the temperature coefficient of the band gap. By the aim of this fact, we estimate the temperature coefficients of the fundamental band gaps for $Al_xGa_{1-x}As$ alloy by using the interpolation scheme between the values of GaAs and AlAs (see Table II).[84]

C. Effective mass

The effective mass, which is strongly connected with the carrier mobility, is known to be one of the most important device parameters.[85] The density-of-state mass m_e in the minima (Γ, X, or L) is obtained from the equation

TABLE II. Electronic band parameters for GaAs, AlAs, and $Al_xGa_{1-x}As$. Validity of the material parameters for $Al_xGa_{1-x}As$ ternary is described in detail in the text.

Parameter	GaAs	AlAs	$Al_xGa_{1-x}As$
Band-gap energy E_g^α (eV)	1.424 (E_g^Γ)[a]	2.168 (E_g^X)[a]	$1.424 + 1.247x$ $(0 \leqslant x \leqslant 0.45)$[a]
			$1.900 + 0.125x + 0.143x^2$ $(0.45 < x \leqslant 1.0)$[a]
Critical-point energy (eV)			
E_0	1.425[b]	3.02[c]	$1.425 + 1.155x + 0.37x^2$[w]
$E_0 + \Delta_0$	1.765[b]	3.32[c]	$1.765 + 1.115x + 0.37x^2$
$E_1(1)$	2.89[b]	3.82[c]	$2.89 + 0.94x$
$E_1(2)$	2.96[b]	3.96[c]	$2.96 + 1.00x$
$E_1(1) + \Delta_1$	3.12[b]	4.03[c]	$3.12 + 0.91x$
$E_1(2) + \Delta_1$	3.19[b]	4.16[c]	$3.19 + 0.97x$
E_0'	4.44[b]	4.54[c]	$4.44 + 0.10x$
$E_0' + \Delta_0'$	4.63[b]	4.69[c]	$4.63 + 0.06x$
E_2	4.99[b]	4.89[c]	$4.99 - 0.10x$
Electron affinity χ_e (eV)	4.07[d]	3.5[d]	$4.07 - 1.1x$ $(0 \leqslant x \leqslant 0.45)$
			$3.64 - 0.14x$ $(0.45 < x \leqslant 1.0)$
Ionicity f_i	0.310[e]	0.274[e]	$0.310 - 0.036x$
Pressure coefficient of E_g^α ($\times 10^{-6}$ ev/bar)			
dE_g^Γ/dP	11.5[f]	10.2[g]	$11.5 - 1.3x$
dE_g^X/dP	-0.8[h]	-0.8[i]	-0.8
dE_g^L/dP	2.8[h]	2.8[i]	2.8
Temperature coefficient of E_g^α ($\times 10^{-4}$ eV/deg)			
dE_g^Γ/dT	-3.95[j]	-5.1[k]	$-3.95 - 1.15x$
dE_g^X/dT	-3.6[l]	-3.6[k]	-3.6
Conduction-band effective mass			
Γ valley m_e^Γ	0.067[a]	0.150[a]	...
X valley m_{tX}	0.23[m]	0.19[n]	...
m_{lX}	1.3[o]	1.1[n]	...
L valley m_{tL}	0.0754[p]	0.0964[q]	...
m_{lL}	1.9[r]	1.9[s]	...
Density-of-states electron mass m_e^α			
Γ valley m_e^Γ	0.067	0.150	$0.067 + 0.083x$
X valley m_e^X	0.85[t]	0.71[t]	$0.85 - 0.14x$
L valley m_e^L	0.56[t]	0.66[t]	$0.56 + 0.1x$
Conductivity effective mass m_c^α			
Γ valley m_c^Γ	0.067	0.150	$0.067 + 0.083x$
X valley m_c^X	0.32[t]	0.26[t]	$0.32 - 0.06x$
L valley m_c^L	0.11[t]	0.14[t]	$0.11 + 0.03x$
Valence-band effective mass			
m_{lh}	0.087[u]	0.150[v]	$0.087 + 0.063x$
m_{hh}	0.62[v]	0.76[v]	$0.62 + 0.14x$
m_{so}	0.15[v]	0.24[v]	$0.15 + 0.09x$

[a] H. C. Casey, Jr. and M.B. Panish, *Heterostructure Lasers* (Academic, New York, 1978), Part A.

[b] M. Cardona, K. L. Shaklee, and F. H. Pollak, Phys. Rev. **154**, 696 (1967).

[c] A. Onton, *Proceedings of the 10th International Conference on the Physics of Semiconductors* (Cambridge, Mass., 1970), p. 107. Note that his symmetry assignment was corrected by W. H. Berninger and R. H. Rediker [Bull. Am. Phys. Soc. **16**, 306 (1971)].

[d] These values are taken from a tabulation of A. G. Milnes and D. L. Feucht [*Heterojunctions and Metal-Semiconductor Junctions* (Academic, New York, 1972)].

[e] J. C. Phillips, *Bonds and Bands in Semiconductors* (Academic, New York, 1973).

[f] R. Zallen and W. Paul, Phys. Rev. **155**, 703 (1967).

[g] Extrapolated from the data of $Al_xGa_{1-x}As$ by N. Lifshitz, A. Jayaraman, R. A. Logan, and R. G. Maines [Phys. Rev. B **20**, 2398 (1979)].

[h] Calculated by D. L. Camphausen, G. A. N. Connell, and W. Paul [Phys. Rev. Lett. **26**, 184 (1971)].

[i] Assumed similar to GaP (see text).

[j] M. Zvara, Phys. Status Solidi **27**, K157 (1968).

[k] B. Monemar, Phys. Rev. B **8**, 5711 (1973).

[l] Assumed that $dE_g^X/dT = dE_2/dT$ (see text). The data of dE_2/dT is taken from R. R. L. Zucca and Y. R. Shen [Phys. Rev. B **1**, 2668 (1970)].

[m] F. H. Pollak, C. W. Higginbotham, and M. Cardona, J. Phys. Soc. Jpn. Suppl. **21**, 20 (1966).

[n] B. Rheinlander, H. Neumann, P. Fischer, and G. Kuhn, Phys. Status Solidi B **49**, K167 (1972).

[o] E. M. Conwell and M. O. Vassell, Phys. Rev. **166**, 797 (1968).

[p] D. E. Aspnes and A. A. Studna, Phys. Rev. B **7**, 4605 (1973).

[q] Calculated from the usual $k \cdot p$ theory (see text).

[r] D. E. Aspnes, Phys. Rev. B **14**, 5331 (1976).

[s] Assumed similar to GaAs.

[t] Calculated from $m_e^\alpha = N^{2/3} m_{t\alpha}^{2/3} m_{l\alpha}^{2/3}$, where N is the number of equivalent α minima ($\alpha = \Gamma$, X, or L). Calculated also from $m_c^\alpha = (2/m_{t\alpha} + 1/m_{l\alpha})^{-1}$.

[u] A. L. Mears and R. A. Stradling, J. Phys. C **4**, L22 (1971).

[v] Taken from a tabulation of P. Lawaetz [Phys. Rev. B **4**, 3460 (1971)].

[w] Taken from H. J. Lee, L. Y. Juravel, J. C. Woolley, and A. J. S. Thorpe, Phys. Rev. B **21**, 659 (1980).

$$m_e^{\alpha} = N^{2/3} m_{t\alpha}^{2/3} m_{l\alpha}^{1/3}, \tag{28}$$

where N is the number of equivalent α minima ($N = 1$ for the Γ minimum, $N = 3$ for the X minima, and $N = 4$ for the L minima) and $m_{t\alpha}$, $m_{l\alpha}$ are the transverse and longitudinal masses of the minima, respectively. The conductivity effective mass m_c^{α} is also given by

$$\frac{1}{m_c^{\alpha}} = \frac{1}{3}\left(\frac{2}{m_{t\alpha}} + \frac{1}{m_{l\alpha}}\right). \tag{29}$$

The effective mass $m_e^{\Gamma}(= m_c^{\Gamma})$ is known to be strongly connected with the lowest direct gap energy [see Eq. (30) and Fig. 22].

There are many investigations on the compositional dependence of the electron effective mass in the alloy systems (e.g., $Ga_xIn_{1-x}As$, $Ga_xIn_{1-x}Sb$, $InAs_{1-x}Sb_x$, $InAs_{1-x}P_x$, $In_{1-x-y}Ga_xAl_yAs$, and $In_{1-x}Ga_xAs_yP_{1-y}$).[86–91] However, to our knowledge, there is no report on $Al_xGa_{1-x}As$ alloy. The recent publication on $In_{1-x}Ga_xAs_yP_{1-y}$ quaternaries[89] has pointed out that the generally acceptable m_e^{Γ} value is a linear relationship with the composition y. Nicholas *et al.*[87] have measured cyclotron resonance and infrared absorption in the complete range of alloys $InAs_yP_{1-y}$ in the region of the direct gap, and have also found that the effective mass is an almost linear function of the composition. This result is in contrast to the prediction of the $k \cdot p$ theory.[89,92] The three-level $k\cdot p$ analysis at $\mathbf{k} = 0$ in the zinc-blende type semiconductors gives

$$\frac{1}{m_e^{\Gamma}} = 1 + \frac{P_{\Gamma}^2}{3}\left(\frac{2}{E_0} + \frac{1}{E_0 + \Delta_0}\right), \tag{30}$$

where P_{Γ}^2 is the interband squared P-matrix element. Thus, they suggested that the discrepancy is thought to arise from a bowing in P_{Γ}^2.[87] The mass m_t in the L minima can also be calculated from the $k\cdot p$ theory. This analysis gives[93]

$$\frac{1}{m_{tL}} = 1 + P_L^2\left(\frac{1}{E_1} + \frac{1}{E_1 + \Delta_1}\right), \tag{31}$$

where E_1 and Δ_1 are the interband gap and spin-orbit splitting energies at the L point, respectively (see Sec. IV A), and P_L^2 is the squared P-matrix element. The value of $m_{tL} = 0.0964 m_0$ for AlAs in Table II is obtained from this expression assuming that the matrix element P_L^2 of this material has the same values as that of GaAs ($P_L^2 = 18.4$ eV).

The electron effective mass is rather accurately known from numerous experiments, but the valence-band (hole) masses must essentially be calculated from band theory. This approach was made by Lawaetz[94] for diamond- and zinc-blende-type semiconductors. There are no experimental data on the compositional dependence of the valence-band masses in the alloy system $Al_xGa_{1-x}As$. Spin-polarized photoluminescence measurement by Hermann and Pearsall[95] suggested that for $In_{1-x}Ga_xAs_yP_{1-y}$ quaternaries lattice-matched to InP, the light-hold mass m_{lh} is an almost linear function of composition y. One can find that the mass m_{lh} is successfully assumed to have the same value as m_e^{Γ}, which is a good approximation in the Kane's model (see Fig. 16). Based on such trends, m_{lh} is assumed to vary linearly between Lawaetz's values for GaAs and AlAs. Similarly,

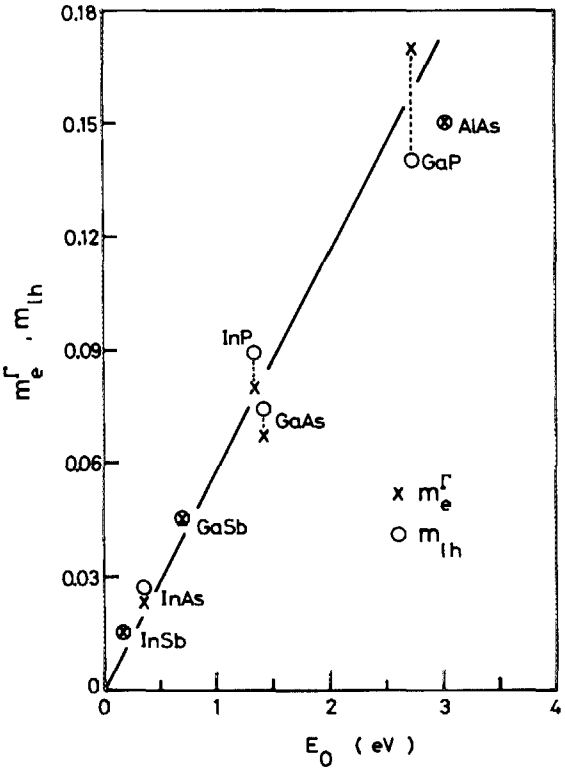

FIG. 16. Effective masses, m_e^{Γ} and m_{lh}, as a function of the lowest-direct gap E_0 for some of the III-V binaries.

m_{hh} (heavy-hole mass) and m_{so} (spin-orbit band mass) are assumed to vary linearly with composition x.

The effective mass plays a quite large role in determining the impurity ionization energy. Let us now check the acceptability of the above-estimated, band-mass parameters from an aspect of the impurity-ionization-energy analysis. The ionization energy of a donor state as a function of x in $Al_xGa_{1-x}As$ alloy was studied by many workers.[96–101] In accordance with the conduction-band structure of $Al_xGa_{1-x}As$ alloy (see Sec. IV A), the character of a shallow donor state could be expected to change from Γ-like ($0 \leqslant x \leqslant 0.45$), via L-like, to X-like ($0.45 < x \leqslant 1.0$) in nature. The unique nature of electronic states associated with an GaAs-$Al_xGa_{1-x}As$ superlattice has also been the subject of a great deal of interest both from the theoretical and experimental viewpoints.[102–105] The simplest calculation of donor ionization energy in a bulk semiconductor is based on the so-called hydrogen approximation (in eV)[106]: $E_I = 13.6(z/\epsilon_s)^2 m_c^{\alpha}$, where Z is the effective charge of the ionized center, ϵ_s the dielectric constant (see Sec. V A), and m_c^{α} is the conductivity electron effective mass [divided by m_0 (free electron mass)]. The hydrogen approximation for the ionization energy for acceptors is similar to that for the donors.

A concomitant gradual change of the impurity state in $Al_xGa_{1-x}As$ alloy can be expected from this expression. The x dependence of the impurity state in $Al_xGa_{1-x}As$ has been studied by mean of luminescence[96] or Hall effect measurements.[97–99] The calculated compositional dependence of the ionization energies in $Al_xGa_{1-x}As$ alloy for the donors

(Γ-, X-, and L-like) and acceptor (top of the valence band at $\mathbf{k}=0$) is shown in Fig. 17 (see also Table IV). The ionization energies for $Al_xGa_{1-x}As$ vary nearly linearly and increase with increasing composition x. The structure of the valence band remains qualitatively unchanged in going from GaAs to AlAs. The variation of the hydrogenic acceptor energy $E_I(V)$ vs x for $Al_xGa_{1-x}As$ shows clear quadratic dependence on composition x. Dingle *et al.*[96] have measured the photoluminescence spectra through the entire compositional range of $Al_xGa_{1-x}As$, and obtained the free and bound excitons and donor-associated luminescence band. The donor-associated band was attributed to variations in the donor ionization energy as a function of x. This result is also plotted in Fig. 17 by the open circles. These data show a quite good agreement with the calculated values except in the region around $x\simeq 0.45$. Below $x\simeq 0.35$ the donor appears very GaAs-like in nature and the dominant contribution to the donor electron work function would come from Bloch functions near $\mathbf{k}=0$ (Γ). Similarly, for $x>0.7$, the dominant contribution would come from about the X-band extrema. If considerably little or no interaction between the Γ and X donor states occurs they will cross sharply at the Γ-X band crossover composition ($x\simeq 0.45$). The experimental data, however, showed a strong peak in this compositional range and, as a result, any sharp crossover did not occur. To describe such an abnormal behavior would require a large interaction (or coupling) between the Γ, L, and X bands in the crossover region.[107] The acceptor energies in Zn-doped p-$Al_xGa_{1-x}As$ were found to increase from $E_I(V)=15$ meV for $x=0$ to 90 meV for $x=0.5$.[108] It is found that these data show a qualitative agreement with the hydrogen approximation but not so good quantitatively. The result was also compared with the effective-mass approximation by Henning *et al.*,[109] and qualitative agreement was achieved. Quantitatively, however, the discrepancy between the experiment and calculation was rather large. The discrepancy should be due to a failure of the simple hydrogen (effective-mass) approximation or ignorance of possible interactions between the valence bands (heavy, light, and spin-orbit bands).

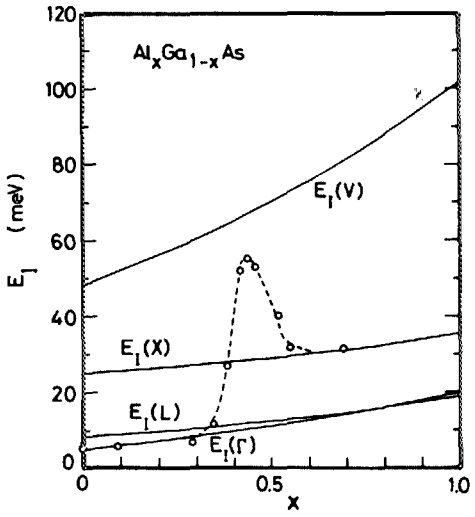

FIG. 17. Donar ionization energies, $E_I(\Gamma)$, $E_I(X)$, and $E_I(L)$, and acceptor ionization energy $E_I(V)$ as a function of composition x for $Al_xGa_{1-x}As$ alloy. The theoretical curves (solid lines) are obtained from the hydrogen approximation using the band-mass parameters estimated in Sec. IV C. The experimental data (open circles) are taken from Ref. 96.

D. Deformation potential

The purpose of this subsection is to estimate and discuss various types of deformation potentials for $Al_xGa_{1-x}As$ alloy. It has been shown that the lattice mobility of holes in III-V compounds is limited primarily by acoustic and nonpolar-optical mode scattering.[18] The strengths of these scattering mechanisms are determined essentially by the valence-band deformation potentials, namely a, b, and d (Pikus–Bir's notation).[110] Fundamental piezo-optical properties, e.g., piezo-birefringence and Raman (Brillouin) scattering, are also strongly affected by these potentials.[111] The orbital strain Hamiltonian for the valence bands at $\mathbf{k}=0$ in the zinc-blende-type crystals can now be written as[110]

$$\mathcal{H}_{ev} = -a(e_{xx}+e_{yy}+e_{zz}) - 3b\left[\left(L_x^2-\frac{1}{3}L^2\right)e_{xx}+\text{c.p.}\right] - \frac{6}{\sqrt{3}}d\left[(L_x,L_y)e_{xy}+\text{c.p.}\right], \tag{32}$$

where e_{ij} denotes the components of the strain tensor, L the angular momentum operator, c.p. denotes cyclic permutations with respect to the rectangular coordinates x, y, z, and the quantities in the square brackets indicate the symmetrized product of $[L_x,L_y]=\frac{1}{2}(L_xL_y+L_yL_x)$, etc. The orbital strain Hamiltonian for the conduction band at $\mathbf{k}=0$ is also given by

$$\mathcal{H}_{ec}=a'(e_{xx}+e_{yy}+e_{zz}). \tag{33}$$

The parameters a and a' are the hydrostatic pressure deformation potentials, and b and d are the shear deformation potentials. Although the shear deformation potentials b and d have been measured for many materials (see Ref. 2), it is difficult to obtain values for the hydrostatic potential a since most experiments measure changes in energy gaps and their related effects rather than absolute shifts of the band edges. However, Lawaetz[112,113] has proposed a theoretical expression based on the dielectric band theory of Phillips which allows a to be estimated with reasonable accuracy. His theory leads to the following expression for a:

$$a=-0.4\frac{E_{vh}^2}{E_v}-0.7\frac{C^2}{E_v}, \tag{34}$$

where a, E_v, E_{vh}, and C are in eV (see notations used in Ref. 113). Expression (34) recalls existence of any relation between the quantity a (b or d) and Phillips's ionicity f_i. Indeed, the plots of a calculated from Eq. (34) versus f_i for some of the covalent and III-V materials showed that there is an increase in a with increasing f_i.[2] The plots of $\eta(=d/\sqrt{3}b)$ vs f_i also showed an increase in η with increasing f_i. Such trends could be well interpreted by a point-ion model proposed by Gavini and Cardona.[114] By the aid of such trends, we can estimate the deformation potentials of AlAs to be $a=2.6$ eV, $b=-1.5$ eV, and $d=-3.4$ eV. The deformation potentials of $Al_xGa_{1-x}As$ alloy can, then, be estimated

by the linear interpolation scheme [since to the limiting values of f_i between 0.274 (AlAs) and 0.310 (GaAs) they can be approximated to vary linearly with f_i]. The numerical values estimated from this procedure are listed in Table III.

Lawaetz[112] has determined an effective acoustic-mode deformation potential, $\Xi_{\rm eff}$, appropriate to low-field transport in p-type materials with Ge-like (zinc-blende) valence bands. This parameter is given by

$$\Xi_{\rm eff}^2 = a^2 + \frac{C_l}{C_t}(b^2 + \frac{1}{2}d^2), \tag{35}$$

where C_l and C_t are spherically averaged elastic coefficients given by

$$C_l = (1/5)(3C_{11} + 2C_{12} + 4C_{44}), \tag{36a}$$

$$C_t = (1/5)(C_{11} - C_{12} + 3C_{44}). \tag{36b}$$

The calculated compositional dependence of $\Xi_{\rm eff}$ vs x can be approximated by a linear relationship with a good accuracy (in eV):

$$\Xi_{\rm eff}(x) = 6.7 - 1.2x, \tag{37}$$

where the elastic constants used are taken from Sec. III D (estimated from our model). The deformation potential $\Xi_{\rm eff}$ can be related to the phenomenological acoustic deformation potential E_{ac} proposed by Wiley and DiDomenico[115] by the equation

$$E_{ac}^2 = \frac{\beta + 2}{6\beta}\Xi_{\rm eff}^2, \tag{38}$$

where $\beta = C_t/C_l$. The dependence of E_{ac} on x is also almost linear relationship (in eV):

$$E_{ac}(x) = 3.6 - 0.7x. \tag{39}$$

There are various studies relating the uniaxial stress effects on the band structure of semiconductors.[116] There has also been studied the stress-related effects on lasing characteristics in AlGaAs/GaAs laser diodes.[117] The lowest direct gaps in the zinc-blende-type semiconductors occur in the center of the Brillouin zone, where it has fourfold (counting the two spin states) E_0 and twofold $E_0 + \Delta_0$ gap. It is known that the uniaxial stress can produce a splitting of the fourfold valence bands due to lattice deformation. The energy-gap shift ΔE_g^Γ (or lasing-energy shift) with the applied stress X can be calculated from Eq. (32). The shift calculated is as follows: $\Delta E_g^\Gamma = 2b(C_{11} - C_{12})^{-1}X$ for the [100] stress, and $\Delta E_g^\Gamma = (d/\sqrt{3})C_{44}^{-1}X$ for the [111] stress (C_{ij}: elastic stiffness constant). The values of ΔE_g^Γ (in meV) with the applied stress (in 10^9 dyn/cm^2) can, then, be numerically expressed for $Al_xGa_{1-x}As$ alloy as

$$\Delta E_g^\Gamma(x,X) = (5.23 - 0.48x)X \tag{40a}$$

for the [100] stress, and

$$\Delta E_g^\Gamma(x,X) = (4.42 - 1.09x)X \tag{40b}$$

for the [111] stress.

The distribution of stess in heterojunction semiconductor structures is a subject of perennial, great interest since

TABLE III. Deformation potential constants for GaAs, AlAs, and $Al_xGa_{1-x}As$. Validity of the material constants for $Al_xGa_{1-x}As$ ternary is described in detail in the text.

Parameter	GaAs	AlAs	$Al_xGa_{1-x}As$
Valence-band deformation potential (eV)			
a	2.7[a]	2.6[a]	$2.7 - 0.1x$
b	-1.7[b]	-1.5[c]	$-1.7 + 0.2x$
d	-4.55[b]	-3.4[c]	$-4.55 + 1.15x$
Effective acoustic deformation potential $\Xi_{\rm eff}$ (eV)	6.7[d]	5.5[d]	$6.7 - 1.2$
Phenomenological deformation potential E_{ac} (eV)	3.6[d]	2.9[d]	$3.6 - 0.7x$
Optical deformation potential d_o (eV)	41[d]	42[d]	$41 + x$
Phenomenological optical deformation potential $E_{\rm NPO}$ (eV)	5.9[d]	5.9[d]	5.9[g]
Intravalley deformation potential E_1^a (eV)			
Γ valley E_1^Γ	6.8[e]	6.3[e]	$6.8 - 0.5x$
X valley E_1^X	-2.5[e]	-2.3[e]	$-2.5 + 0.2x$
L valley E_1^L	0.23[e]	0.55[e]	$0.23 + 0.32x$
Intervalley deformation potential field D_{ij} (eV/cm)			
$D_{\Gamma X}$	$(0.5\text{–}1.1)\times10^9$[f]	?	?
$D_{\Gamma L}$	$(0.15\text{–}1.0)\times10^9$[f]	?	?
D_{XL}	$(0.34\text{–}1.1)\times10^9$[f]	?	?
D_{XX}	$(0.27\text{–}1.1)\times10^9$[f]	1.47×10^9[f]	?
D_{LL}	1×10^9[f]	?	?

[a] J. D. Wiley, Solid State Commun. **8**, 1865 (1970).
[b] M. Chandrasekhar and F. H. Pollak, Phys. Rev. B **15**, 2127 (1977).
[c] Estimated in the present study (see text).
[d] Calculated as described in the text.
[e] Estimated from the data of dE_g^a/dP (see text).
[f] There are no precision data up to date. These values are gathered from various sources: G. H. Glover, J. Appl. Phys. **44**, 1295 (1973); P. J. Vinson, C. Pickering, R. A. Adams, W. Fawcett, and G. D. Pitt, *Proceedings of the International Conference on the Physics of Semiconductors* (Tipogravia, Rome, 1976), p. 1243; A. R. Adams, P. J. Vinson, and C. Pickering, Electron. Lett. **13**, 46 (1977); T. J. Maloney and J. Frey, J. Appl. Phys. **48**, 781 (1977); M. A. Littlejohn, J. R. Hauser, and T. H. Glisson, J. Appl. Phys. **48**, 4587 (1977); J. Pozela and A. Reklaitis, Solid State Electron. **23**, 927 (1980); A. K. Saxena and K. S. Gurumurthy, J. Phys. Chem. Solids **43**, 801 (1982); T. L. Koch, L. C. Chin, C. Harden, and A. Yariv, Appl. Phys. Lett. **41**, 6 (1982); and C. L. Collins and P. Y. Yu, Phys. Rev. B **30**, 4501 (1984).
[g] This material parameter shows a very weak nonlinearity with respect to x (see Fig 20).

internal stresses arise normally in thin epitaxail films during preparation of the films by heteroepitaxial growth.[118] The stresses have an important influence on the physical properties of the films. Much attention has, therefore, been paid to the calculation of stress distributions in epitaxial structures[119,120] and, more recently, to heterojunction laser structures.[121,122] Let us now proceed to clarify some relations between the deformation potentials and internal strains in heteroepitaxial films. Rozgonyi *et al.*[123] have carried out evaluation of the internal stress and dislocations in LPE (liquid-phase epitaxial) layers of $Al_xGa_{1-x}As$ on GaAs substrates by using an x-ray topographic camera. They have found that the average stresses in $Al_xGa_{1-x}As$ layers vary linearly with x according to the relation of $X = 2.23x$ (X in 10^9 dyn/cm^2). Ziel and Gossard[124] have measured the energy difference ΔE_g^{Γ} between the light-hold and heavy-hole involved transitions to be 5.7 meV for $Al_{0.5}Ga_{0.5}As$ layer grown on (001) GaAs. Introducing this energy value into Eq. (40a), one can easily estimate the internal stress in the $Al_{0.5}Ga_{0.5}As$ layer. In Fig. 18, the obtained stress is shown by the solid circle, as well as the experimental result of Rozgonyi *et al.* (solid line).[123] An excellent agreement between this calculation and experimental result can be obviously found in the figure. Thus, the relation of Eq. (40) can be used to evaluate the internal stress in $Al_xGa_{1-x}As$/GaAs heterostructure wafers.

The phonons which usually dominate in the scattering probability are the long-wavelength optical phonons. The long-wavelength optical phonons produce a short-range potential in the crystal which shifts the electronic band states. In polar semiconductors, the phonons are also accompanied by a long-range macroscopic electric field which produces additional scattering. The shifts of the electronic band states per unit ionic displacement associated with a long-wavelength optical phonons are called optical deformation potentials. The deduction of the optical deformation potentials from either transport[18] or Raman data[111] is quite involved. Pötz and Vogl[125] have recently presented a systematic theoretical study on the optical deformation potentials for a large class of semiconductors.

Figure 19 shows the plots of the optical deformation potential d_0 versus Phillips's ionicity f_i for some of the covalent and zinc-blende materials. The data are gathered from many sources (e.g., from Refs. 125–128). Although the data are scattered from material to material, the general trend is obvious, i.e., there is a tendency that d_0 decreases with increasing f_i. This is in contrast to the trends of a and $\eta(=d/\sqrt{3}b)$,[2] where they increase gradually with increasing f_i. The value of d_0 for $Al_xGa_{1-x}As$ alloy is assumed to vary linearly with x (see Fig. 20). It has been shown that, to first order, electrons with spherically symmetric wave functions have no deformation-potential interaction with optical phonons.[129] The simplest case of electron–nonpolar-optical-phonon interaction involves the electrons in nondegenerate ellipsoidal conduction bands as found in n-Si and n-Ge. In this case, the nonpolar-optical deformation potential E_{NPO} can be related to d_0 by the following equation[18]:

$$E_{NPO} = \frac{M_1 + M_2}{2(M_1 + M_2)^{1/2}} \left(\frac{C_1(\beta + 2)}{2g\omega_{LO}^2 a^2 \beta} \right)^{1/2} d_0, \tag{41}$$

where M_1 and M_2 are the masses of the atoms in the unit cell, g the crystal density (see Sec. III A), ω_{LO} ($\langle\omega_{LO}\rangle$; see Sec. III D) the frequency of zone-center ($\mathbf{k} = 0$) LO phonons, and a is the lattice constant (see Sec. III A). In Fig. 20, the calculated values of E_{NPO} as a function of x for $Al_xGa_{1-x}As$ alloy are shown along with those of d_0.

Let us now consider the case of scattering of electrons

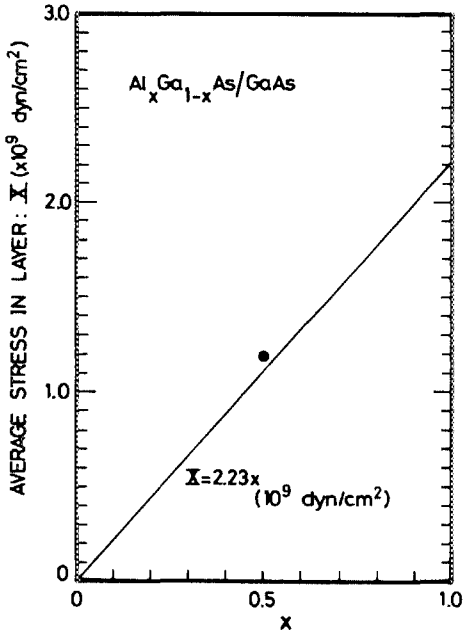

FIG. 18. Average film stress vs composition x for $Al_xGa_{1-x}As$ epitaxial film grown on (100)GaAs. A solid circle is the calculated result (see text).

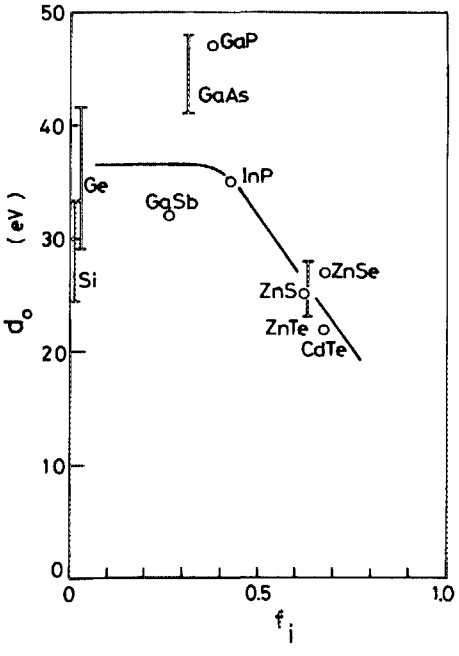

FIG. 19. Plots of d_0 vs Phillips's ionicity f_i for some of the covalent and zinc-blende materials.

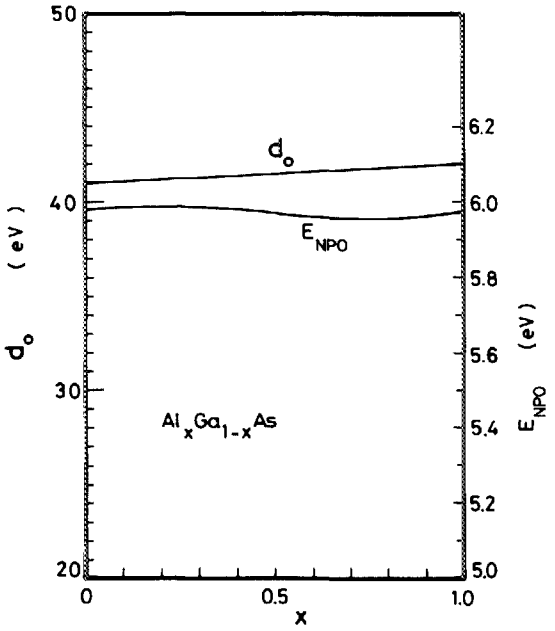

FIG. 20. Optical deformation potential d_0 and nonpolar-optical deformation potential, E_{NPO}, as a function of x for $Al_xGa_{1-x}As$ alloy.

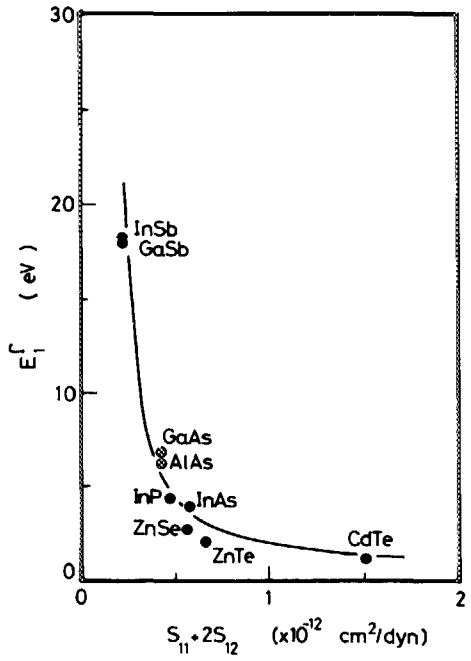

FIG. 21. Trends in E_1^Γ (intravalley deformation potentials) as a function of $(S_{11} + 2S_{12})$ for some of the III-V and II-VI binaries (see text).

due to the strain caused by the acoustic waves, i.e., the intravalley (acoustic) deformation potential scattering. If the strains involved are small as in the usual case, the electronic energy shifts caused by them may be described adequately with linear terms in the strain. By symmetry, for spherical constant energy surfaces and acoustic-mode scattering, one may write for the shift of the conduction-band edge ΔE_{ca} as[130]

$$\Delta E_{ca} = E_1(e_{xx} + e_{yy} + e_{zz}), \tag{42}$$

where $e_{ii}(i = x, y, \text{or } z)$ is the diagonal component of the strain tensor, and E_1 is the so-called intravalley (acoustic) deformation potential. Equation (42) is based on that the matrix element of Eq. (33) is practically equal to that obtained by replacing $\mathscr{H}_{ec}$ by ΔE_{ca}. The deformation potential E_1 can now be written in a phenomenological form as

$$E_1^\alpha \simeq (dE_{ca}^\alpha/dP)/d(S_{11} + 2S_{12}), \tag{43}$$

where dE_{ca}^α/dP is the hydrostatic pressure coefficient of the conduction-band edge (see Sec. IV B) and S_{ij} is the elastic compliance constant. Following the expression of Eq. (43), we plot in Fig. 21 E_1^Γ (Γ-valley electron) against "$(S_{11} + 2S_{12})$" for a number of the III-V and II-VI compounds. The general trend is also obvious, i.e., E_1 decreases abruptly with increasing $(S_{11} + 2S_{12})$. This can be explained by the fact that in Eq. (43) the values of $(S_{11} + 2S_{12})$ varies strongly by material to material while the pressure coefficient dE_{ca}^Γ/dP does not.

Champhausen *et al.*[77] have extended Van Vechten–Phillips's dielectric theory[10] to calculate pressure coefficients of interband energy differences and obtained an excellent agreement with experiment. From the calculated absolute shift of the band edge (L valley) in Ge, they have also obtained the value of E_1 which is found to be acceptable for the deformation potential of this material. Introducing the numerical values of dE_{ca}^α/dP (Sec. IV B and Ref. 131) and S_{ij} (Sec. III D) into Eq. (43), we can estimate the quantities of E_1^α ($\alpha = \Gamma, X,$ or L) as a function of x for $Al_xGa_{1-x}As$ alloy. The results obtained vary almost linearly with composition x (see Table III). Recently, Saxena and Gurumurthy[132] have estimated various scattering parameters from an analysis of the electron mobility in $Al_xGa_{1-x}As$ alloy. The compositional dependence of E_1 obtained in this subsection shows a good agreement with their result. However, a considerable disagreement can be found in the case of E_1^X especially at a region of larger x values. Since not much information could be obtained about this parameter, the exact determination of E_1 is rather more difficult at the present time.

It is generally accepted that the Gunn effect arises from a negative conductance mechanism, in which electrons are transferred from a low-mass central valley (Γ valley) to higher-lying large mass satellite valley (L and/or X valley), such as exist in the conduction band of GaAs. The strength of this electron transfer mechanism can be represented by the coupling constant D_{ij}.[130] The constant D_{ij} ($i,j = \Gamma, X,$ or L) is the so-called intervalley deformation-potential field, and is in units of eV/cm, where $i = j$ corresponds to the equivalent intervalley scattering and $i \neq j$ corresponds to the nonequivalent one. Although the scattering processes play an important role in the analysis of electron-transfer properties, there are no reliable data and theoretical model on these parameters to date. The numerical values listed in Table III are gathered from various sources.

V. COLLECTIVE EFFECTS AND RESPONSE CHARACTERISTICS

A. Static and high-frequency dielectric constants

The concept of the dielectric behavior of solids is an old one which is important for several electron-device proper-

ties.[106] Measurements of the static dielectric constant ϵ_s of GaAs have yielded widely different values ranging from 9.8 to 13.2 at room temperature.[133] The constant ϵ_s can be written as

$$\epsilon_s = \epsilon_\infty + \frac{4\pi N e_T^2}{\omega_{TO}{}^2 M},$$
$$\equiv \epsilon_\infty + S_T, \tag{44}$$

where ϵ_∞ is the high-frequency dielectric constant measured at frequencies well above the long-wavelength longitudinal phonon frequency (ω_{LO}) but below the optical absorption edge, M the reduced mass of the crystal, N the number of unit cells per unit volume, e_T the effective charge, and ω_{TO} is the long-wavelength transverse-optical phonon frequency. The dielectric constants ϵ_s and ϵ_∞ are related to the optical-phonon frequencies by the Lyddane–Sachs–Teller relation:

$$\epsilon_s/\epsilon_\infty = (\omega_{LO}/\omega_{TO})^2. \tag{45}$$

Samara[133] has recently obtained the dielectric constants of GaAs to be $\epsilon_s = 13.18$ and $\epsilon_\infty = 10.89$. Fern and Onton[134] have also reported that for AlAs ϵ_∞ is determined to be 8.16 and the resulting ϵ_s is 10.06. With the known values of ω_{LO}, ω_{TO} (see Sec. III D), and ϵ_s, ϵ_∞ (quoted above), we find that the relation of Eq. (45) is well obeyed for both GaAs and AlAs. We already studied in Ref. 2 general properties of the dielectric constants ϵ_s and ϵ_∞ for a specific family of compounds, namely the III-V and II-VI compounds, and concluded that the constants of their alloys could be deduced by the use of the linear interpolation method. The values of ϵ_s and ϵ_∞ for $Al_xGa_{1-x}As$ alloy are, thus, the results of the linear interpolation scheme (see Table IV).

B. Magnetic susceptibility

Magnetic properties of a given material could be characterized by the corresponding magnetic susceptibility χ_m. This is generally independent of temperatures in diamagnets but varies inversely with the absolute temperature in paramagnets ($\chi_m = C/T$; Curie's law). χ_m is represented in a form by[135,136]

$$\chi_m = \chi_c + \chi_v + \chi_p, \tag{46}$$

where χ_c is the core-electron diamagnetism, χ_v is a Langevin-type diamagnetic component due to the valence electrons which is sensitive to the spatial extent of the valence charge density, and χ_p is a Van Vleck-type paramagnetic interband component arising from the virtual magnetic dipole transition between filled valence- and empty conduction-band states. The susceptibility χ_m can, thus, be theoretically treated as a form similar to that for the dielectric susceptibility,[135] i.e., the dielectric susceptibility is also strongly connected with the core and valence electrons[137] and the virtual dipole transitions between the valence- and conduction-band states.[1] The dielectric susceptibility of an alloy system is well interpreted in terms of the linear interpolation scheme (see, e.g., Sec. V A and V F). From this fact, we can tentatively estimate χ_m of the alloy system $Al_xGa_{1-x}As$ by the linear interpolation between the values of GaAs and AlAs. The binary data used here are taken for GaAs from Ref. 135 and for AlAs from Ref. 136.

C. Piezoelectric constant

An important aspect of the zinc-blende arrangement is the absence of a center of symmetry or inversion. The III-V

TABLE IV. Summary of dielectric, magnetic, and electromechanical response parameters for GaAs, AlAs, and $Al_xGa_{1-x}As$. Optical-transition related constants are also summarized in this table.

Parameter	GaAs	AlAs	$Al_xGa_{1-x}As$
Static dielectric constants ϵ_s	13.18[a]	10.06[b]	$13.18 - 3.12x$
High-frequency dielectric constant ϵ_∞	10.89[a]	8.16[b]	$10.89 - 2.73x$
Magnetic susceptibility χ_m ($\times 10^{-5}$ cm^3/mole)	-3.33[c]	-2.51[d]	$-3.33 + 0.82x$
Piezoelectric constant e_{14} (C/m^2)	-0.16[e]	-0.225[f]	$-0.16 - 0.065x$
d_{14} ($\times 10^{-12}$ m/V)	-2.69[g]	-3.82[g]	$-2.69 - 1.13x$
Electromechanical coupling constant K_{14}	0.0617[g]	0.094[g]	$0.0617 + 0.0323x$
Fröhlich coupling constant α_F			
Γ valley	0.068[h]	0.126[g]	$0.068 + 0.058x$
X valley	0.152[g]	0.166[g]	$0.152 + 0.014x$
Donor ionization energy (meV)			
Γ valley $E_I(\Gamma)$	5.2[i]	20.2[i]	$5.2 + 7.9x + 7.1x^2$
X valley $E_I(X)$	24.8[i]	35.3[i]	$24.8 + 7.06x + 3.44x^2$
L valley $E_I(L)$	8.7[i]	19.0[i]	$8.7 + 5.8x + 4.5x^2$
Acceptor ionization energy $E_I(V)$ (meV)	48.5[i]	102.0[i]	$48.5 + 30.2x + 23.3x^2$
Net charge Q (eV)	0.46[j]	0.47[j]	$0.46 + 0.01x$
Exciton Rydberg energy G (meV)	4.7[g,k]	17.0[g]	$4.7 + 6.82x + 5.48x^2$
Exciton Bohr radius a_B (Å)	115[g]	42[g]	$115 - 142x + 61x^2$

[a] G. A. Samara, Phys. Rev. B 27, 3494 (1983).
[b] R. E. Fern and A. Onton, J. Appl. Phys. 42, 3499 (1971).
[c] S. Hudgens, M. Kastner, and H. Fritzsche, Phys. Rev. Lett. 33, 1552 (1974).
[d] T. Sahu and P. K. Misra, Phys. Rev. B 26, 6795 (1982).
[e] G. Arlt and P. Quadflieg, Phys. Status Solidi 25, 323 (1968).
[f] K. Hübner, Phys. Status Solidi B 57, 627 (1973).
[g] Calculated as described in the text.
[h] J. T. Devreese, *Polarons in Ionic Crystals and Polar Semiconductors* (North-Holland, Amsterdam, 1977).
[i] Calculated as described in the text (see Sec. IV C).
[j] C. A. Coulson, L. B. Redei, and D. Stocher, Proc. R. Soc. London 270, 357 (1962).
[k] M. A. Gilleo, P. T. Bailey, and D. E. Hill, Phys. Rev. 174, 898 (1968).

compounds crystallizing in the zinc-blende structure are the simplest crystals lacking a center of symmetry and, hence, capable of exhibiting piezoelectric and related effects depending on polar symmetry. The piezoelectric tensor in the zinc-blende crystals ($F\bar{4}3m$) has the form[22]:

$$\mathbf{e} = \begin{bmatrix} 0 & 0 & 0 & e_{14} & 0 & 0 \\ 0 & 0 & 0 & 0 & e_{14} & 0 \\ 0 & 0 & 0 & 0 & 0 & e_{14} \end{bmatrix}, \tag{47}$$

i.e., it has only one tensor component e_{14}. The piezoelectric effects are significant for the study of transport properties in semiconductors.[18,85]

The piezoelectric scattering of electrons in semiconductors is usually not of major practical importance, except in high-quality crystals, because of impurity scattering. At low temperatures ($\lesssim 50$ K), however, lattice scattering of electrons is known to be dominated by the piezoelectric interaction, which causes elastic scattering due to the relatively low-energy acoustic phonons.[85] We shall first sketch the piezoelectric constants of specific family of binary compounds, namely the III-V and II-VI compounds, from a simplified point of view.

Piezoelectricity is the generation of electronic polarization by application of stress to a crystal lacking a center of symmetry. Arlt and Quadflieg[138] have measured piezoelectric constants for a variety of materials and have proposed the microscopic origins of piezoelectricity as being due to such as ionic polarization, strain-dependent ionicity, and electronic polarization. Many theoretical works[139–142] have also been performed to understand piezolelectric properties in crystals on the basis of the lattice-dynamic treatment by adding the concept of the ionicity scale derived by Phillips.[76] The plots of e_{14} versus Phillips's ionicity f_i for some of the III-V and II-VI compounds are shown in Fig. 22. The data

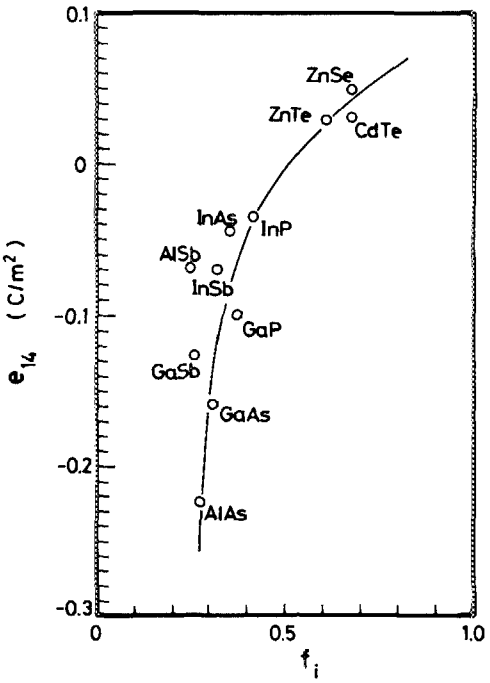

FIG. 22. Plots of e_{14} vs Phillips's ionicity f_i for some of the III-V and II-VI binaries.

are taken from Refs. 138, 140, and 143. One can easily understand from the figure that e_{14} of materials passes through zero at $f_i \simeq 0.5$ while undergoing a reversal in sign. Hübner[140] has predicted the piezoelectric constants for a number of the III-V, II-VI, I-VII compounds and found to be in good numerical agreement with correct sign with experimental data.

The piezoelectric constant e_{14} of $Al_xGa_{1-x}As$ alloy is thought to be successfully estimated by the linear interpolation method. This is based on the fact that to the limiting values of f_i, as in the case of GaAs ($f_i = 0.310$)-AlAs($f_i = 0.274$), e_{14} could be approximated to vary linearly with f_i (see Fig. 22). The interpolated values of e_{14}, as a function of x, can now be given by (in C/m^2)

$$e_{14}(x) = -0.16 - 0.065x. \tag{48}$$

The piezoelectric component $d_{k,ij}$, which has the same tensor form as Eq. (47), is connected reciprocally with the tensor component $e_{k,mn}$ through

$$d_{k,ij} = \sum_{mn} S_{ijmn} e_{k,mn}, \tag{49}$$

where S_{ijmn} is the elastic compliance constant discussed in Sec. III D. In the case of the zinc-blende crystals, the tensor $\mathbf{d}$ can be expressed only by the component d_{14}:

$$d_{14} = S_{44} e_{14}. \tag{50}$$

The calculated value of d_{14}, as a function of x, is also almost linear relationship give by (in 10^{-12} m/V)

$$d_{14}(x) = -2.69 - 1.13x. \tag{51}$$

It is known[144] that injected ultrasonic waves can be amplified in piezoelectric semiconductors by the application of a sufficiently high electric field because of the strong interaction with mobile charge carriers. Domains of intense acoustic flux, showing a broad band of frequencies in the low-GHz range, can also be produced in piezoelectric semiconductors, such as GaAs[145] and GaSb,[146] by acoustoelectric amplification of phonons from the thermal equilibrium spectrum. The gain of such acoustoelectric interactions can be explained in terms of the material parameter K^2, called the electromechanical coupling constant.[144] The carrier mobilities in semiconductors are also strongly affected by this parameter.[85] The coupling constant K^2 is a crystal-direction-dependent quantity. The maximum coupling of the transverse acoustic waves is along the [110] direction for the zinc-blende type crystal, which is the reason why the majority of experiments have been carried out with crystals cut in this direction.[144–146] In this case, the coupling constant can be written as

$$K_{14}^2 = \frac{e_{14}^2}{\epsilon_s C_{44}}, \tag{52}$$

where e_{14} is the piezoelectric constant, ϵ_s the dielectric constant (see Sec. V A), and C_{44} is the elastic stiffness constant (see Sec. III D). The calculated value of K_{14} for $Al_xGa_{1-x}As$ alloy, as a function of x, is an almost linear relationship given by

$$K_{14}(x) = 0.0617 + 0.0323x. \tag{53}$$

The value of K_{14}^2 as a function of x, on the other hand, is

given by a quadratic form:

$$K_{14}^2(x) = (3.81 + 3.99x + 1.04x^2) \times 10^{-3}. \quad (54)$$

D. Fröhlich coupling parameter

It is known that the coupling between the electron and longitudinal-optical (LO) lattice vibrations cannot be neglected in the study of transport and optical properties in polar semiconductors.[85] A measure of the interaction between the electron and LO phonons can be represented by the well-known Fröhlich coupling constant[147]:

$$\alpha_F = \frac{1}{2} \frac{e^2/(\hbar/2m^*\omega_{LO})^{1/2}}{\hbar\omega_{LO}} \left(\frac{1}{\epsilon_\infty} - \frac{1}{\epsilon_s} \right). \quad (55)$$

One can see that this constant depends strongly on the ionic polarization of the crystal which is related to the dielectric constants ϵ_∞ and ϵ_s (see Sec. V A). The high-frequency dielectric constant ϵ_∞ is accurately determined by measuring the wavelength dependence of the refractive index.[134] The quantities ϵ_s and ϵ_∞ are related to the optical-phonon frequencies by the Lyddane–Sachs–Teller relation [see Eq. (45)]. The Debye temperature of the LO phonon frequency is an important parameter in the study of the polaron mobility at finite temperatures (see Sec. V E). This temperature is defined by

$$\theta_{po} = \hbar\omega_{LO}/k, \quad (56)$$

where k is the Boltzmann constant. The last parameter we need in order to consider the coupling constant α_F is the electron effective mass m^*. This mass corresponds to the conductivity effective band mass defined by Eq. (29) (see Sec. IV C). In the case of polar semiconductors, a Faraday-rotation experiment permits a direct measurement of the conduction band mass (Γ-valley mass). One suspects from such arguments the presence of a relation between the crystal ionicity and coupling constant α_F. Figure 23 shows the plots of α_F versus Phillips's ionicity f_i for some of the III-V and II-VI compounds. The data quoted are gathered from the text book (Ref. 147). The constant α_F increases gradually with increasing f_i. This is the general trend of α_F.

Because of the lack of experimental data, we have to restrict ourselves to obtain α_F of $Al_xGa_{1-x}As$ alloy by a numerical calculation. Equation (55) leads us to get numerical estimation of α_F. Figure 24 shows the results of this calculation. The material parameters used are taken for m^* ($= m_c^\alpha$) from Sec. IV C, for ϵ_s and ϵ_∞ from Sec. V A, and for $\hbar\omega_{LO}$ from Sec. III D. The detailed theory of the Fröhlich interactions in alloys where there are two-mode LO phonons present has not been reported previously. Because of this reason, we used in the present study the effective phonon energy $\langle\omega_{LO}\rangle$ defined in Sec. III D instead of the single phonon energy ω_{LO} (GaAs-like or AlAs-like). The calculated compositional dependence of α_F vs x is approximated by linear relationships:

$$\alpha_F(x) = 0.068 + 0.058x \quad (57a)$$

for the Γ-valley electrons, and

$$\alpha_F(x) = 0.152 + 0.014x \quad (57b)$$

for the X-valley electrons.

The electron–LO-phonon coupling is known to modify the electron effective band mass.[147] One of the ways to get information about m^* is a cyclotron resonance experiment. However, this experiment gives the polaron mass rather than the band mass. For GaAs this correction is expected to be of the order of 1% in the bulk crystal.[148] The band mass can be computed by means of Langreth's formula[149]

$$m^* = [(1 - 0.0008\alpha_F^2)/(1 - \alpha_F/6 + 0.0034\alpha_F^2)]m, \quad (58)$$

where m is the cyclotron mass known from experiment. The calculated correction factor $m_{pol}^\Gamma/m_e^\Gamma$ [m_{pol}^Γ: polar mass; m_e^Γ: band mass (see Sec. IV C) as a function of x for $Al_xGa_{1-x}As$

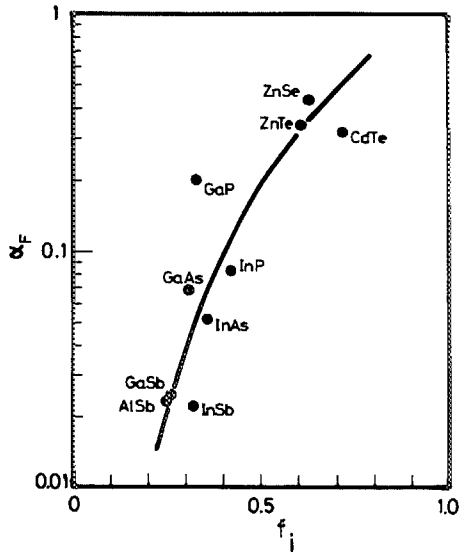

FIG. 23. Plots of α_F vs Phillips's ionicity f_i for some of the III-V and II-VI binaries.

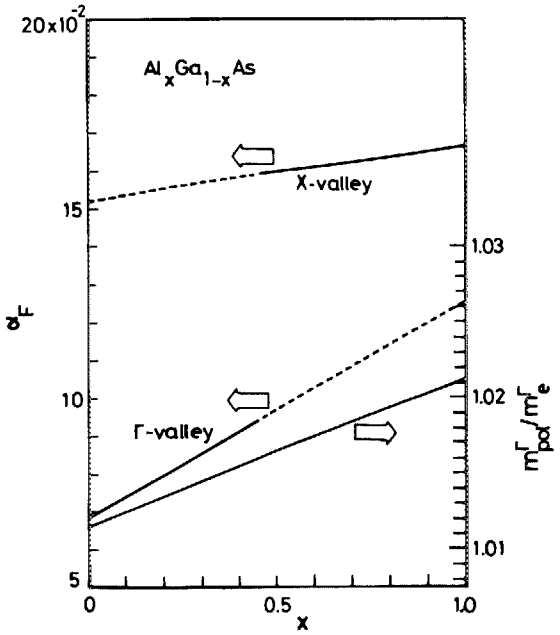

FIG. 24. Fröhlich coupling constant α_F in the Γ and X valleys of $Al_xGa_{1-x}As$ as a function of composition x. The compositional dependence of the polar-mass correction factor is also shown in the figure (see text).

alloy is also plotted in Fig. 24. This polaron correction is found to increase almost linearly with increasing x.

E. Electron transport properties

Although $Al_xGa_{1-x}As$ has important electron- and microwave-device applications, little information is available about the electron transport properties in this alloy system.[132,150–153] This is due to the lack of knowledge of exact variation of the basic material parameters (such as electron effective mass, polar optical phonon energy, and deformation potentials) with composition x and, thus, it is not completely justified to compare the measured transport coefficients (mobilities) with calculated ones. The electron mobility is a popular parameter used to characterize the microscopic quality of semiconductors.[85] Accurate comparisons between experiment and calculation are of great importance for determining a variety of fundamental material parameters and electron scattering mechanisms. There are various electron scattering mechanisms, such as polar optical scattering, deformation-potential scattering, piezoelectric scattering, intervalley scattering, impurity scattering, and alloy scattering. Our knowledge of the material parameters discussed in Sec. III-V enables to calculate the strengths of various scattering mechanisms (except alloy scattering) in the conduction-band minima (Γ, X, or L) as a function of x for $Al_xGa_{1-x}As$ alloy. In polar semiconductors like $Al_xGa_{1-x}As$, longitudinal optical modes have an associated electric polarization field. The strength of this field can be written in a form as

$$E_0 = \frac{m^* e\omega_{LO}}{\hbar}\left(\frac{1}{\epsilon_\infty} - \frac{1}{\epsilon_s}\right). \tag{59}$$

This field E_0 is the so-called effective polar field. In this subsection, we try to calculate the electron mobilities in $Al_xGa_{1-x}As$ alloy which are limited only by the polar optical scattering. The polar optical scattering is the dominant mechanism near room temperature in direct-gap semiconductors. In alloy semiconductors, there is also increasing need to better understand electron scattering due to the random alloy potentials of the crystalline lattice. This type of scattering mechanism (i.e., alloy scattering) is also discussed in this subsection.

For high-field devices of $Al_xGa_{1-x}As$, it is necessary to know the electron mobility (or velocity) and electric-field characteristics of the alloys for each composition. The optical phonon energies $\hbar\omega_{LO}$ of III-V compounds are comparable or larger than thermal energy kT at room temperature and, as a result, the polar optical scattering must include the inelastic nature in any quantitative theory. When the scattering mechanism is elastic, as in impurity scattering, a relaxation time characterizing the rate at which momentum decay can be defined. From the relaxation time, one can calculate the perturbation of an equilibrium electron distribution by a small electric field and, hence, the mobility. When the scattering is inelastic, no relaxation time exists exactly, although in certain limits this approximation can be useful. The Boltzmann transport expression in which the average rates of energy loss and momentum loss through collisions are balanced by energy and momentum gain due to the electric field provides the following energy and momentum balance equations[130]:

$$\left\langle\frac{d\epsilon}{dt}\right\rangle_E + \sum_i \left\langle\frac{d\epsilon}{dt}\right\rangle_i = 0, \tag{60a}$$

$$\left\langle\frac{dp}{dt}\right\rangle_E + \sum_i \left\langle\frac{dp}{dt}\right\rangle_i = 0, \tag{60b}$$

where the index i refers to the ith scattering mechanism, and the subscipt E refers the electric field.

Let us now consider a simple case in which energy loss of electrons comes from only polar optical scattering. As mentioned before, this scattering is the most dominant mechanism near room temperature in direct-gap semiconductors. For a Maxwell–Boltzmann distribution at electron temperature T_e, the average rates of change of carrier energy and momentum due to polar optical interactions are readily found to be[130]

$$\left\langle\frac{d\epsilon}{dt}\right\rangle_{po} = \left(\frac{2k\theta_{po}}{\pi m^*}\right)^{1/2} eE_0 \frac{e^{(\chi_0-\chi_e)}-1}{e^{\chi_0}-1}\chi_e^{1/2}e^{\chi_e/2}K_0(\chi_e/2), \tag{61a}$$

$$\left\langle\frac{dP}{dt}\right\rangle_{po} = \frac{2eE_0N_q}{3(\pi)^{1/2}}\frac{(m^*)^{1/2}v_d}{(2k\theta_{p0})^{1/2}}\chi_e^{3/2}e^{\chi_e/2} \times\left[(e^{(\chi_0-\chi_e)}+1)K_1(\chi_e/2) + (e^{(\chi_0-\chi_e)}-1)K_0(\chi_e/2)\right], \tag{61b}$$

where m^* ($= m_e^\Gamma$) is the electron effective mass at the Γ valley, E_0 the effective polar field given by Eq. (59), θ_{po} the Debye temperature of the LO phonon frequency defined by Eq. (56), $\chi_e = \hbar\omega_{LO}/kT_e$, $\chi_0 = \hbar\omega_{LO}/kT_0$ with T_0 lattice temperature, $N_q = (e^{\chi_0}-1)^{-1}$, v_d the electron drift velocity in the electric field E, and K_0 and K_1 are modified Bessel functions of the second kind. The equations for the changes in energy and momentum due to the applied electric field are given by

$$\left\langle\frac{d\epsilon}{dt}\right\rangle_E = ev_dE, \tag{62a}$$

$$\left\langle\frac{dp}{dt}\right\rangle_E = eE. \tag{62b}$$

Introducing Eqs. (61) and (62) into Eq. (60), we obtain the electron mobility μ_{po} limited by the polar optical scattering as

$$\mu_{po} = \left[\frac{m^*\chi_eE^2}{3k\theta_{po}}\frac{(e^{(\chi_0-\chi_e)}+1)K_1(\chi_e/2)+(e^{(\chi_0-\chi_e)}-1)K_0(\chi_e/2)}{(e^{(\chi_0-\chi_e)}-1)K_0(\chi_e/2)}\right]^{-1/2}. \tag{63}$$

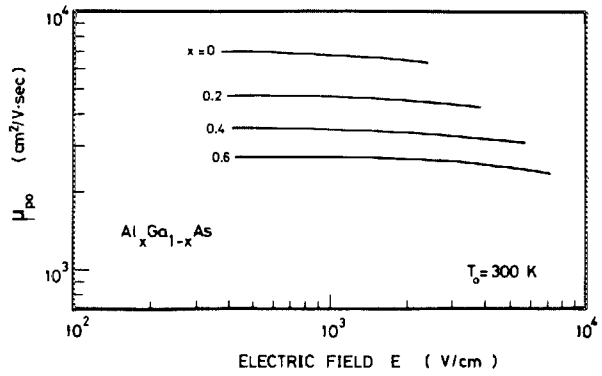

FIG. 25. Polar-optical-scattering-limited mobility μ_{po} as a function of electric field intensity E for $Al_xGa_{1-x}As$ alloy at $T_0 = 300$ K.

The electric field-electron temperature ($E - T_e$) relation can also be given by

$$(E/E_0)^2 = \frac{2}{3\pi} N_q^2 \chi_e^2 e^{\chi_e} (e^{(\chi_0 - \chi_e)} - 1) K_0(\chi_e/2) \times [(e^{(\chi_0 - \chi_e)} + 1) K_1(\chi_e/2) + (e^{(\chi_0 - \chi_e)} - 1) K_0(\chi_e/2)]. \quad (64)$$

Figure 25 shows the calculated results of the electron mobility μ_{po} at lattice temperature of $T_0 = 300$ K as a function of the electric field E with x(Al)-composition increments of 0.2. The corresponding E-T_e relation is also shown in Fig. 26. The numerical values used are taken for m^* ($= m_e^\Gamma$) from Sec. IV C, for E_0 (ϵ_s and ϵ_∞) from Sec. V A, and for $\hbar\omega_{LO}$ from Sec. III D. Due to the two-LO-phonon nature in $Al_xGa_{1-x}As$ (see Sec. III D), one can expect that the electron-phonon interactions vary in a complex way for this alloy system. There are various theoretical calculations of low-field electron mobility using some kinds of interpolation scheme.[154] To take into account the two-LO-phonon effects, we introduced the effective LO-phonon energy $\langle\hbar\omega_{LO}\rangle$ instead of one-phonon energy $\hbar\omega_{LO}^G$ or $\hbar\omega_{LO}^A$. The calculated

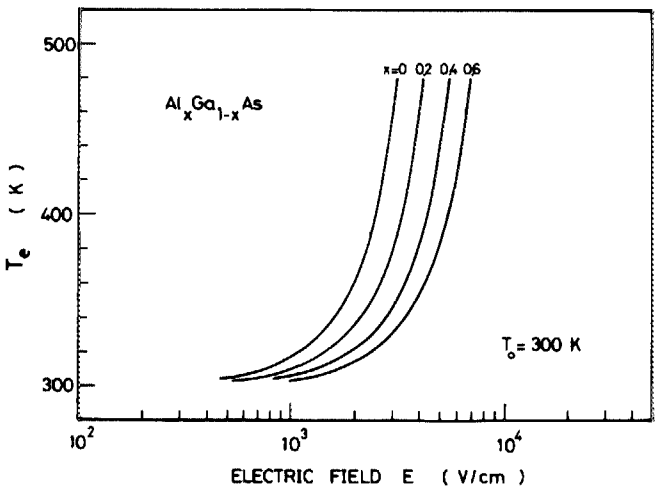

FIG. 26. Electron temperature T_e as a function of electric field intensity E for $Al_xGa_{1-x}As$ alloy at $T_0 = 300$ K.

mobility μ_{po} decreases gradually with increasing E. The electron temperature T_e, vice versa, increases with increasing E. It is also clear that μ_{po} decreases definitely with increasing composition x. It may be expected that experimental mobility, if one measured, would decrease drastically at higher field region ($E \gtrsim 10^3$ V/cm for $x = 0$) because of the onset of nonequivalent ($\Gamma - X$, $\Gamma - L$) intervalley scattering in this field region.[155,156] This type of scattering process could not be solved in a simple analytical form and, therefore, was not taken into account in our calculations. Possibly the most accurate modeling to date of such an analysis is a Monte-Carlo particle simulation.[157] This simulation promises to provide an exact method for the evaluation of transport coefficients under quantum conditions, and is based on various scattering parameters (physical constants) regarding the microscopic behavior of the electrons in semiconductor. However, one notices that it is sometimes difficult to check the validity of such scattering parameters [e.g., intervalley deformation-potential field D_{ij} (see Sec. IV D)].

It is expected that when we increase the external electric field the carrier velocity will increase in accordance with the relation $v = \mu E$ (μ: mobility). The "saturated" drift velocity of the carriers tends to limit the expected performance of various semiconductor devices. For GaAs,[158] the electrons reach a peak velocity of $v_d = 2.2\times10^7$ cm/s for $E \simeq 3$ kV/cm before intervalley transfer occurs from the Γ to the L (X) valley and, then, decrease to the saturated values of $\sim 1\times10^7$ cm/s for an ordinary electric field $E \simeq 10$ kV/cm. Let us estimate the saturated electron velocities in the Γ, X, and L minima of $Al_xGa_{1-x}As$ alloy. If one assumes that a single high-energy phonon (long-wavelength LO phonon) dominates the energy relaxation, the expected saturated velocity v_{es} can be written as[159]

$$v_{es}^\alpha = (8\hbar\langle\omega_{LO}\rangle/3\pi m_c^\alpha)^{1/2}, \quad (65)$$

where m_c^α is the conductivity effective mass in the α (Γ, X, or L) valley (see Sec. IV C). If several scattering mechanisms are present, then the expression is far more complicated, as can be recognized from Eq. (60). In Fig. 27, the calculated results of Eq. (65) are plotted as a function of composition x. The saturated electron velocity in the central valley decreases drastically with increasing x, but those in the X and L valleys increase slightly. The expected saturated velocity v_{es}^Γ in GaAs ($\sim 3\times10^7$ cm/s) is larger than the experimental peak velocity (2.2×10^7 cm/s).[158] However, the calculated v_{es} in the satellite valley of GaAs is comparable to the experimental saturated velocity ($\sim 1\times10^7$ cm/s). It can, thus, be considered that in GaAs the Γ-valley electrons exhibit a peak velocity before reaching the phonon-limited electron velocity (v_{es}^Γ) caused by the onset of intervalley transfer, then the velocity is limited by the satellite-valley saturated one.

In alloy semiconductors, such as $Al_xGa_{1-x}As$, the electrons see potential fluctuations due to the compositional disorder. This effect produces a peculiar scattering mechanism, namely alloy scattering.[160–162] The alloy-scattering potential is considered to be due to the polarization deviation caused by the deviation of effective charge arising from the deviation in the electronegativity of atoms caused by the deviation of the covalent radius.[150] The ionic compounds have

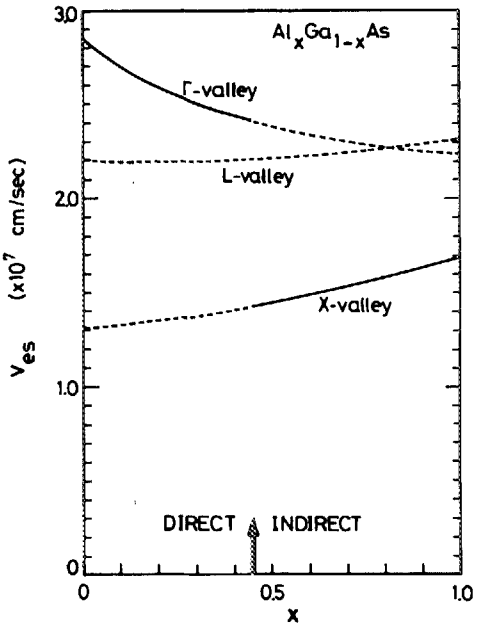

FIG. 27. Saturated electron velocities in the Γ, X, and L minima of $Al_xGa_{1-x}As$ alloy as a function of composition x.

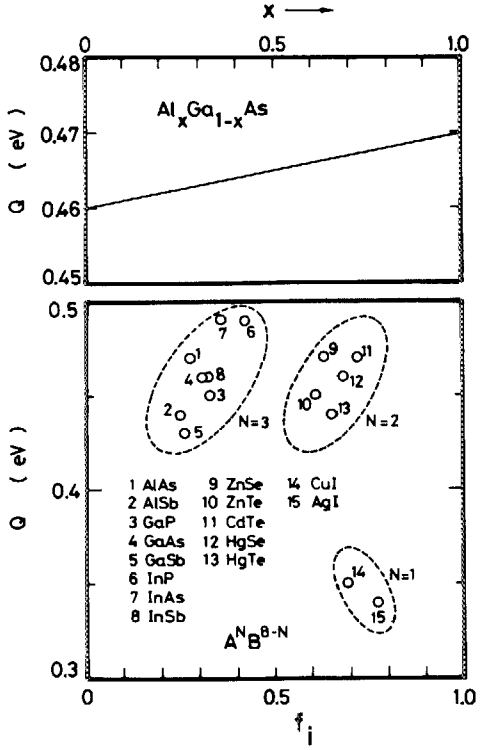

FIG. 28. Plots of net charge Q vs Phillips's ionicity f_i for a wide variety of A^NB^{8-N} type compounds. The interpolated net charge Q for $Al_xGa_{1-x}As$ versus x is also shown in the top of this figure.

ionic bonding and, thus, have a net charge Q. Figure 28 shows a variation of Q versus Phillips's ionicity f_i for a wide variety of A^NB^{8-N}-type compounds. The data are taken from a tabulation of Coulson *et al.*[163] It is clear that the net charge Q can be classified into groups in terms of the cation number N, as shown by the dashed circles. The interpolated net charge for $Al_xGa_{1-x}As$ versus x is also shown in the top of this figure. The alloy-scattering potential ΔE_a can be obtained from this net charge, and the mobility μ_{al} in the Γ valley of $Al_xGa_{1-x}As$ limited to the alloy scattering mechanism is expressed as[150]

$$\mu_{al} = \frac{52.83 T_e^{-1/2}}{(m_e^{\Gamma})^{5/2} x(1-x)(\Delta E_a)^2}. \tag{66}$$

This expression leads to partial mobility decreasing as $(m_e^{\Gamma 5} T_e)^{-1/2}$. The $T_e^{-1/2}$ dependence is well known,[161] and the $(m_e^{\Gamma})^{-5/2}$ dependence is consistent with experimental results on alloy semiconductors. The calculated mobilities μ_{al} for $Al_xGa_{1-x}As$ at $T_e = 77$ and 300 K are shown in Fig. 29. This mobility shows a minimum in the alloy composition $x \simeq 0.7$. A comparison of this result with that of Fig. 25 also suggests that the alloy scattering does not play an important part at higher temperature (300 K). The polar-optical and alloy-scattering limited mobilities discussed in this subsection are only typical examples, but are thought to be useful in considering the fundamentals of transport properties in $Al_xGa_{1-x}As$ alloy. Carrier mobilities limited by various kinds of scattering mechanisms (e.g., deformation-potential scattering, piezoelectric scattering, etc.) can also be calculated using the corresponding scattering parameters as determined in the present study.

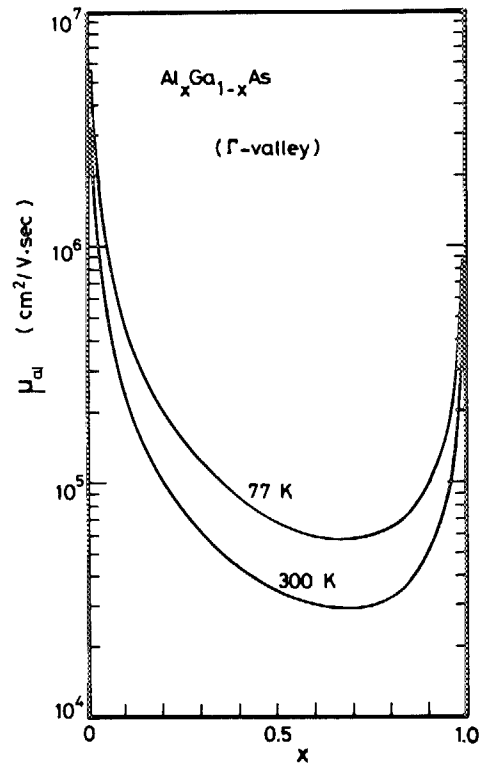

FIG. 29. Alloy-scattering-limited mobility μ_{al} in the Γ minimum as a function of composition x for $Al_xGa_{1-x}As$ alloy.

F. Optical properties

The purpose of this subsection is to make clear fundamental optical properties of $Al_xGa_{1-x}As$ alloy. The pheno-

menon of excitons in crystals has been a subject of considerable interest for many years and has been summarized, e.g., by Knox,[164] and in particular with respect to the group III-V compounds by Dimmock.[165] The exciton state and its behaviors are known to be well characterized by the exciton Rydberg energy G (in eV):

$$G = \frac{\mu e^4}{2\hbar^2 \epsilon_s^2} = 13.6 \frac{\mu}{\epsilon_s^2}, \tag{67}$$

where μ is the exciton reduced mass. The exciton Bohr radius a_B (in Å) can now be given by

$$a_B = \frac{\hbar^2 \epsilon_s}{\mu e^2} = 0.53 \epsilon_s / \mu. \tag{68}$$

Let us first sketch the exciton Rydberg energy G of specific family of binary compounds, III-V and II-VI compounds, from a simplified point of view. Figure 30 shows the plots of G versus E_0 (lowest-direct gap energy) for a number of the III-V and II-VI compounds. It is easily understood from this figure that higher E_0-gap material has larger G value. From a plot of m_e^Γ or ϵ_s vs E_0,[2] we can find the following generalized relationships (see also Fig. 15):

$$m_e^\Gamma \simeq 0.06 E_0, \tag{69}$$

$$\epsilon_s \simeq -3.2 E_0 + 19.0. \tag{70}$$

Assuming $m_e^\Gamma \simeq \mu$ and introducing Eqs. (69) and (70) into Eq. (67), we can obtain the value of G as a function of E_0. The solid line in Fig. 30 is the result of this calculation. It is found that this theoretical curve shows a good agreement with the experimental data (solid circles).

The calculated exciton Rydberg energy G and Bohr radius a_B as a function of x for $Al_xGa_{1-x}As$ can be written as

$$G\,(\text{meV}) = 4.7 + 6.82x + 5.48x^2, \tag{71}$$

$$a_B(\text{Å}) = 115 - 142x + 61x^2. \tag{72}$$

These numerical values exhibit considerable bowing for both G and a_B. Gilleo *et al.*[166] have determined the Rydberg energy for GaAs ($G = 4.7$ meV) from photoluminescence measurement. Our result agrees quite well with this experiment. The intensity of the exciton spectrum is known to be strongly affected by damping, i.e., by a lifetime broadening. The damping effect should be influenced by the alloy disorder, as well as the lattice thermal vibrations and defects.[167,168] Henning and Strehlow[167] have, however, shown theoretically that this contribution is negligibly small in the case of the III-V alloy crystals.

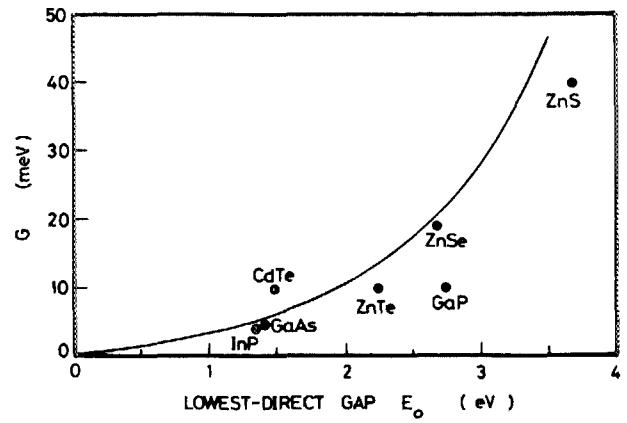

FIG. 30. Exciton Rydberg energy G as a function of the lowest-direct-gap energy E_0 for some of the III-V and II-VI binaries. The solid line is calculated dependence of G on E_0 (see text).

The properties of heterojunctions that permit much lower threshold current densities than homostructure lasers can best be illustrated with the double heterostructure.[61,117] One of the most important factors in heterostructure lasers and optoelectronic devices are the refractive index. In the previous paper,[1] we presented a model for calculation of refractive indices in III-V compounds at energies below the direct band edge. The theoretical prediction shows a quite good agreement with the existing experimental data of III-V binaries and $In_{1-x}Ga_xAs_yP_{1-y}$ quaternaries. In the following, we try to estimate the refractive indices of $Al_xGa_{1-x}As$ based on our model.[1]

The real part of the dielectric constant $\epsilon_1(\omega)$ in the zinc-blende material below the direct band edge can be expressed as[1]

$$\epsilon_1(\omega) = A_0\{f(\chi) + \tfrac{1}{2}[E_0/(E_0+\Delta_0)]^{3/2} f(\chi_{so})\} + B_0, \tag{73}$$

with

$$f(\chi) = \chi^{-2}[2 - (1+\chi)^{1/2} - (1-\chi)^{1/2}], \tag{74}$$

$$\chi = \hbar\omega / E_0, \tag{75}$$

$$\chi_{so} = \hbar\omega / (E_0 + \Delta_0). \tag{76}$$

In Eqs. (73)–(76), A_0 and B_0 are constants and $\hbar\omega$ is the photon energy. The constants A_0 and B_0 can be determined by fitting Eq. (73) with the experimental data. Casey *et al.*[169] have measured the refractive indices of $Al_xGa_{1-x}As$ for AlAs mole fractions between $0 \leqslant x \leqslant 0.38$. The refractive index of AlAs has also been determined by Fern and Onton.[134] The constants A_0 and B_0 as a function of composition x, as determined by least-square fitting Eq. (73) with these experimental data, are found to be written as

$$A_0(x) = 6.3 + 19.0x, \tag{77a}$$

$$B_0(x) = 9.4 - 10.2x. \tag{77b}$$

Introducing the numerical values of A_0, B_0 [Eq. (77)], E_0, $E_0 + \Delta_0$ (see Sec. IV A) into Eq. (73), one can easily calculate the spectral dependence of ϵ_1 in the $Al_xGa_{1-x}As$ alloy system with an optional composition x. Since the imaginary part of the dielectric constant may be taken as zero in the region of the lowest-direct gap, one also obtains the frequency-dependent refractive index $n(\omega)$ in the relation:

$$n(\omega) \simeq \epsilon_1(\omega)^{1/2}. \tag{78}$$

The calculated refractive indices of this system as a function of the photon energy with x-composition increments of 0.1 are shown in Fig. 31. The refractive index step between GaAs and $Al_xGa_{1-x}As$ can also be calculated numerically in the same manner (Fig. 32). One must, however, take care that this calculation would provide good effective-phase indices but less accurate values for group indices in waveguiding devices.[170]

G. Photoelastic properties

In this subsection, we shall present the spectral depen-

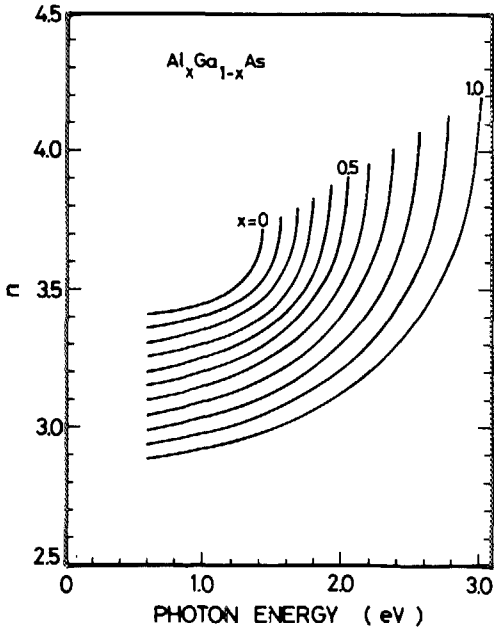

FIG. 31. Calculated refractive indices of $Al_xGa_{1-x}As$ as a function of the photon energy with x-composition increments of 0.1.

dence of photoelastic constants in the $Al_xGa_{1-x}As$ alloy system. Knowledge of the photoelastic constants forms an important part not only in the calculation of the figure of merit for some kinds of the optoelectronic devices[171] but also in the analysis of heteroepitaxial wafers based on the crystal optics.[4]

The application of an external uniaxial stress to a solid produces a change in its crystal symmetry which results in

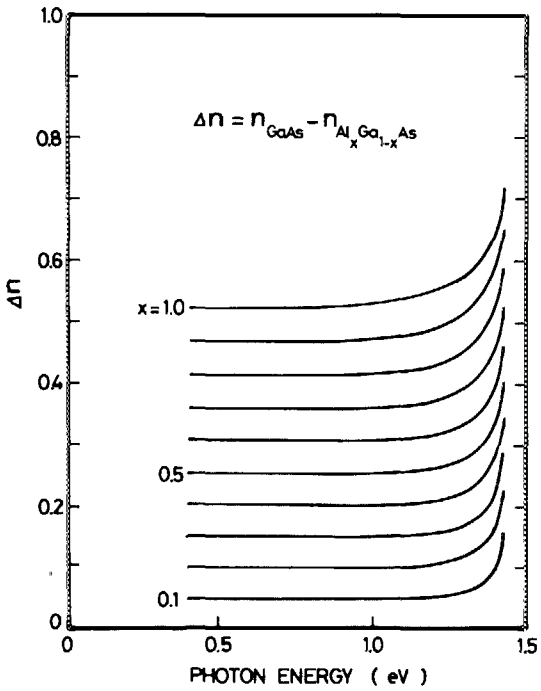

FIG. 32. Refractive-index steps between GaAs and $Al_xGa_{1-x}As$ as a function of the photon energy with x-composition increments of 0.1.

significant changes in its optical properties. An optically isotropic semiconductor becomes birefringent under the action of this stress. This stress effect can be expressed as

$$\frac{\Delta\epsilon_{ij}}{X} = -\sum_{mn} \epsilon_{ii}\epsilon_{jj}p_{ijkl}S_{klmn}, \tag{79}$$

where $\epsilon_{ij} = \epsilon_{\parallel} - \epsilon_{\perp}$ is the charge in the real part of the dielectric constants parallel and perpendicular to the direction of the applied stress X, p_{ijkl} the component of the fourth-rank photoelastic tensor [same form as Eq. (7)], and S_{klmn} is the component of the elastic compliance tensor. The photoelastic constant p_{ijkl} [$(p_{11} - p_{12})$ for $X \parallel [100]$ or p_{44} for $X \parallel [111]$] can now be written as[4]

$$p_{ijkl} = C_0\left\{-g(\chi) + \frac{4E_0}{\Delta_0}\left[f(\chi) - \left(\frac{E_0}{E_0+\Delta_0}\right)^{3/2} f(\chi_{so})\right]\right\} + D_0, \tag{80}$$

with

$$C_0\begin{cases} = -\frac{1}{\epsilon_1^2}\left(\frac{3}{2}\mu\right)^{3/2}P^2 b E_0^{-5/2} & \text{for } X \parallel [100], \quad (81a) \\ = -\frac{1}{\epsilon_1^2}\left(\frac{3}{2}\mu\right)^{3/2}P^2 d E_0^{-5/2} & \text{for } X \parallel [111], \quad (81b) \end{cases}$$

$$g(\chi) = \chi^{-2}[2 - (1+\chi)^{-1/2} - (1-\chi)^{-1/2}], \tag{82}$$

where μ is the combined-density-of-states mass at Γ point, P^2 the squared P-matrix element (see Sec. IV C), and b and d are the shear deformation potentials of the valence band (see Sec. IV D). In Eq. (80), the first term corresponds to the dispersive contribution arising from the E_0 and $E_0 + \Delta_0$ gaps and the second term D_0 corresponds to the nondispersive contribution arising from other, far-off critical points in the band structure (see, e.g., Fig. 13). Ziel and Gossard[124] have measured the internal-stress-induced change in the refractive index $\Delta n = n_{\parallel} - n_{\perp}$ $[= \frac{1}{2}\epsilon_1^{-1/2}(\epsilon_{\parallel} - \epsilon_{\perp})]$ for $Al_xGa_{1-x}As$ ($x \simeq 0.5$) epitaxial layer on (001)GaAs substrate. Based on our procedure reported recently,[4] we can obtain the spectral dependence of $p_{11} - p_{12}$ for $Al_{0.5}Ga_{0.5}As$. The fitting parameters C_0 and D_0 for $Al_{0.5}Ga_{0.5}As$ are determined as follows: $C_0 = -0.25$ and $D_0 = 1.19$. The numerical values of C_0 and D_0, as a function of x, for $Al_xGa_{1-x}As$ can now be given by the equations (see Appendix B)

$$C_0(x)\begin{cases} = -0.46 + 0.42x & \text{for } X \parallel [100], \quad (83a) \\ = -0.21 + 0.19x & \text{for } X \parallel [111], \quad (83b) \end{cases}$$

$$D_0(x)\begin{cases} = 2.22 - 2.05x & \text{for } X \parallel [100], \quad (84a) \\ = 2.12 - 1.95x & \text{for } X \parallel [111], \quad (84b) \end{cases}$$

The band-gap energies E_0 and $E_0 + \Delta_0$ are also specified in terms of x alone (see Table II). Introducing these expressions into Eq. (80), we can obtain the spectral dependence of the photoelastic constants of $Al_xGa_{1-x}As$ alloy with optional composition x. The calculated photoelastic constants of this alloy as a function of the photon energy with x-composition increments of 0.2 for the cases of the stress parallel to the [100] and [111] axes are shown in Figs. 33 and 34, respectively. One can recognize from the figures that the photoelastic constants of $Al_xGa_{1-x}As$ have strong wavelength depen-

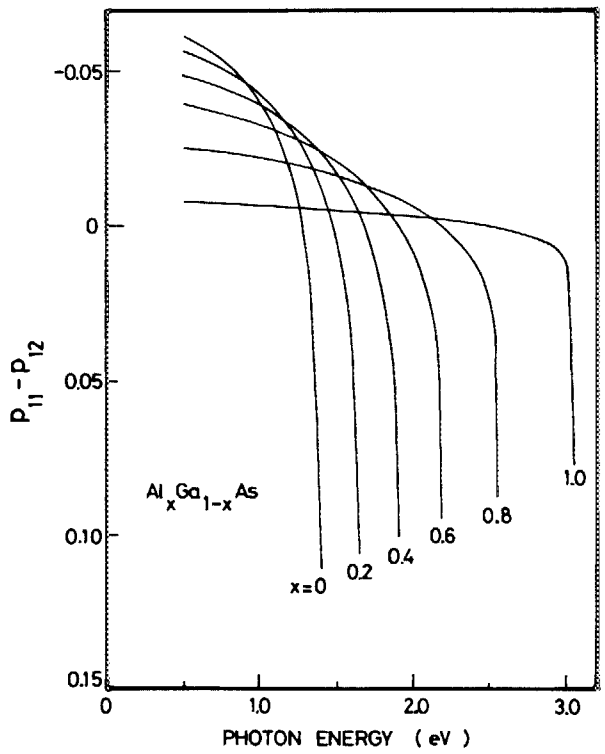

FIG. 33. Calculated photoelastic constant $p_{11}-p_{12}$ for $Al_xGa_{1-x}As$ as a function of the photon energy with x-composition increments of 0.2.

dence. The longer-wavelength photoelastic constant decreases with increasing composition x. As the photon energy approaches the lowest-direct gap, the constant increases drastically.

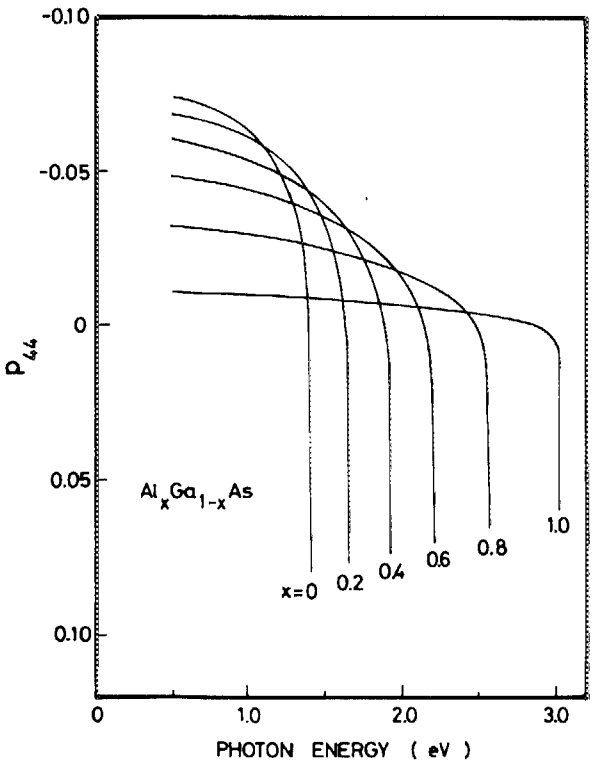

FIG. 34. Calculated photoelastic constant p_{44} for $Al_xGa_{1-x}As$ as a function of the photon energy with x-composition increments of 0.2.

VI. CONCLUSION

The $Al_xGa_{1-x}As$/GaAs system has been the subject of considerable research and device development activity over the past years. A number of important semiconductor properties of $Al_xGa_{1-x}As$ for their analysis require quite detailed and precise knowledge of material parameters, but it is at present rather difficult to obtain the most reliable values from the literature reported. Various models for calculation of physical parameters in compound alloys are discussed, and the results for $Al_xGa_{1-x}As$ ternary alloy are presented. An interpolation scheme has been used for want of any more detailed experimental data, and that the accuracy of the interpolated values are probably estimates of this alloy. It is found that the present model provides generally acceptable parameters, in good agreement with the existing experimental data. The material parameters obtained are also used with wide success to make clear fundamental material properties of this alloy. Of particular interest is the deviation of material parameters from linearity with respect to composition x. Some material parameters, such as lattice constants, crystal density, thermal expansion coefficient, dielectric constant, and elastic constant, obey Vegard's rule well. The parameters, e.g., electronic-band energy, lattice vibration (phonon) energy, Debye temperature, and impurity ionization energy, exhibit quadratic dependence upon composition x. Some kinds of material parameters, e.g., lattice thermal conductivity, on the other hand, exhibit very strong nonlinearity with respect to x which arises from the effects of alloy disorder. A detailed discussion is also given of the acceptability of the interpolated parameters in connection with the solid-state physics. Key properties of the material parameters for a variety of $Al_xGa_{1-x}As$ device applications are also discussed in detail.

ACKNOWLEDGMENTS

The author wishes to thank Dr. K. Kumabe for his continual encouragement. The author also would like to acknowledge useful discussions with all members of the Physical Science Section 2, Musashino ECL, NTT.

APPENDIX A: SURFACE-ACOUSTIC WAVES IN $Al_xGa_{1-x}As$ ALLOY

The purpose of this Appendix is to estimate a set of the elastic constants from the analysis of surface-acoustic-wave velocity v_{sw} in $Al_xGa_{1-x}As$ alloy. The theoretical velocity of v_{sw} is given by Eq. (15). There has, however, been found a considerable disagreement between the experimental data and calculated velocities obtained from a complete set of the elastic constants of ours and Keyes's model (see Sec. III D). Let us now define an elastic constant C_a

$$C_a \equiv C_{11} \simeq \tfrac{1}{2}C_{12} \simeq \tfrac{1}{2}C_{44}. \tag{A1}$$

One can easily recognize the validity of this simple assumption for most of the III-V, zinc-blende-type crystals. The calculated velocity variation versus C_a for AlAs is plotted in Fig. 35 along with the corresponding experimental data $v_{sw}^{[100]}$ and $v_{sw}^{[110]}$ (dashed lines). The elastic constant C_a which

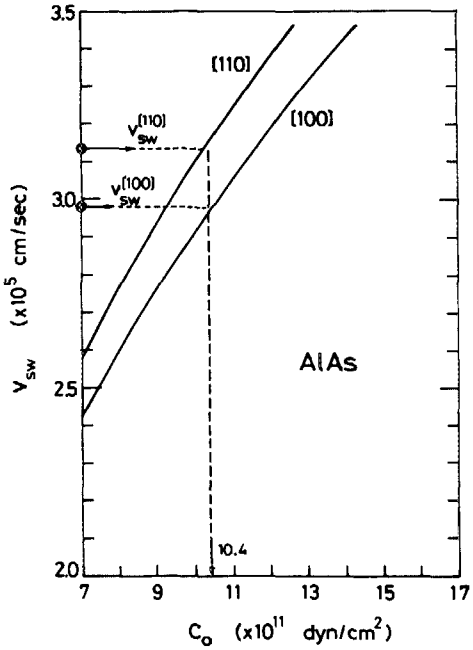

FIG. 35. Calculated surface-acoustic velocity (v_{sw}) variation vs elastic constant C_a for AlAs along with the corresponding experimental data (Ref. 28).

coincides well with the experimental data is found from this figure to be 10.4×10^{11} dyn/cm^2. The constant C_{ij} for AlAs is thus determined to be $C_{11}=10.4$, $C_{12}=5.2$, and $C_{44}=5.2\times10^{11}$ dyn/cm^2. The values of C_{ij} as a function of x for $Al_xGa_{1-x}As$ are, then, calculated taking a linear interpolation between GaAs (Table I) and AlAs as (in 10^{11} dyn/cm^2)

$$C_{11}=11.88-1.48x, \tag{A2a}$$

$$C_{12}=5.38-0.18x, \tag{A2b}$$

$$C_{44}=5.94-0.74x. \tag{A2c}$$

Introducing Eq. (A2) into Eq. (15) and taking into account the density variation, we can obtain the compositional dependence of v_{sw} for $Al_xGa_{1-x}As$ alloy. This result is shown in Figs. 8 and 9 by the dotted lines. Agreement between this calculation and experiment is quite good. However, the elastic constants of AlAs and resulting those of $Al_xGa_{1-x}As$ alloy differ considerably from ours and also from Keyes's values (Sec. III D). This problem is, therefore, still open to experimental verification. From an aspect of this point of view, it is interesting to determine the compositional dependence of C_{ij} for $Al_xGa_{1-x}As$ alloy.

APPENDIX B: DETERMINATION OF C_0 AND D_0 FOR CALCULATION OF THE PHOTOELASTIC CONSTANTS

This determination is based on a linear interpolation scheme and, therefore, necessitates known values for the related binaries GaAs and AlAs. These values are listed in Table V. The values of C_0 and D_0 for GaAs were determined by least-square fitting the experimental data (Ref. 172) with Eq. (80). There is no experimental data on AlAs. The values C_0 and D_0 for $X\|[100]$ of AlAs can be predicted from a linear extrapolation between the data of GaAs and $Al_{0.5}Ga_{0.5}As$ (see Sec. V G) to be $C_0=-0.04$ and $D_0=0.17$. In our

TABLE V. Numerical values of C_0 and D_0 for GaAs and AlAs.

Stress		GaAs	AlAs
$X\|\|[100]$	C_0	-0.46^a	-0.04^b
	D_0	2.22^a	0.17^b
$X\|\|[111]$	C_0	-0.21^a	-0.02^c
	D_0	2.12^a	0.17^c

[a]Determined from the least-square fit of Eq. (81) to the experimental data. [C. W. Higginbotham, M. Cardona, and F. H. Pollak, Phys. Rev. **184**, 821 (1969)].
[b]Obtained from a linear extrapolation between the data of GaAs and $Al_{0.5}Ga_{0.5}As$ (see text).
[c]Estimated (see text).

previous study (Ref. 4), we tried to find some relations between the best-fit parameters (C_0 and D_0) and the lowest-direct gap energy E_0 for a number of the III-V compounds. It was found that the parameters C_0 decreases asymptotically with increasing E_0, in other words, C_0 has the largest value for the smallest E_0-energy material. From this simple trend, one can estimate the value C_0 for $X\|[111]$ of AlAs to be -0.02. The parameter D_0, on the other hand, did not show such a simple relation with the E_0-gap energy. As pointed out in the text, the long-wavelength, nondispersive parameter D_0 includes the contributions from the higher-lying gaps, such as E_1, $E_1+\Delta_1$, and E_2. Long-wavelength dielectric properties of semiconductors have been treated successfully by Van Vechten (Ref. 173) and Yu *et al.* (Ref. 174) with the Penn gap model. Based on their analyses and our earlier result (Ref. 4), we can carry out a rough prediction that for AlAs D_0 for $X\|[111]$ has nearly the same value as that for $X\|[100]$. The expressions of Eqs. (83) and (84) are obtained by using the linear interpolation between these values.

[1]S. Adachi, J. Appl. Phys. **53**, 5863 (1982).
[2]S. Adachi, J. Appl. Phys. **53**, 8775 (1982).
[3]S. Adachi, J. Appl. Phys. **54**, 1844 (1983).
[4]S. Adachi and K. Oe, J. Appl. Phys. **54**, 6620 (1983).
[5]S. Adachi and K. Oe, J. Appl. Phys. **56**, 74 (1984).
[6]S. Adachi and K. Oe, J. Appl. Phys. **56**, 1499 (1984).
[7]G. H. Olsen, T. Z. Zamerowski, R. T. Smith, and E. P. Bertin, J. Electron. Mater. **9**, 977 (1980).
[8]H. Sonomura, H. Horinaka, and T. Miyauchi, Jpn. J. Appl. Phys. **22**, L689 (1983).
[9]J. A. Van Vechten and T. K. Bergstresser, Phys. Rev. B **1**, 3351 (1970).
[10]J. C. Phillips and J. A. Van Vechten, Phys. Rev. Lett. **22**, 705 (1969).
[11]J. C. Phillips, in *Treatise on Solid State Chemistry*, edited by N. B. Hannay (Plenum, New York, 1973), Vol. 1, p. 1.
[12]H. Kressel and H. Nelson, in *Physics of Thin Films*, edited by G. Hass, M. H. Francombe, and R. W. Hoffman (Academic, New York, 1973), Vol. 7, p. 115.
[13]C. M. H. Driscoll, A. F. W. Willoughby, J. B. Mullin, and B. W. Straughan, in *Gallium Arsenide and Related Compounds* (Inst. of Phys., London, 1975), p. 275.
[14]M. Ettenberg and R. J. Paff, J. Appl. Phys. **41**, 3926 (1970).
[15]J. Whitaker, Solid-State Electron. **8**, 649 (1965).
[16]M. C. Rowland and D. A. Smith, J. Crystal Growth **38**, 143 (1977).
[17]L. R. Weisberg and J. Blanc, J. Appl. Phys. **34**, 1002 (1963).
[18]J. D. Wiley, in *Semiconductors and Semimetals*, edited by R. K. Willardson and A. C. Beer (Academic, New York, 1975), Vol. 10, p. 91.
[19]M. B. Panish, J. Crystal Growth **27**, 6 (1974).
[20]M. B. Panish and M. Ilegems, in *Progress in Solid State Chemistry*, edited by H. Reiss and J. O. McCaldin (Pergamon, Oxford, 1972), Vol. 7, p. 39.

[21]I. Kudman and R. J. Paff, J. Appl. Phys. **43**, 3760 (1972).
[22]J. F. Nye, *Physical Properties of Crystals* (Clarendon, Oxford, 1972).
[23]R. W. Keyes, J. Appl. Phys. **33**, 3371 (1962).
[24]H. B. Huntington, *The Elastic Constants of Crystals* (Academic, New York, 1958).
[25]R. V. G. S. Rao, Current Sci. (India) **16**, 91 (1947).
[26]M. S. Kushwaha, Phys. Rev. B **24**, 2115 (1981).
[27]See, for example, G. W. Farnell, in *Physical Acoustics*, edited by W. P. Mason and R. N. Thurston (Academic, New York, 1970), Vol. 6, p. 109.
[28]J. Sapriel, J. C. Michel, J. C. Tolédano, R. Vacher, J. Kervarec, and A. Regreny, Phys. Rev. B **28**, 2007 (1983). Note that there is a typographical error in Eq. (5) of this reference.
[29]F. W. Voltmer, E. P. Ippen, R. M. White, T. C. Lim, and G. W. Farnell, Proc. IEEE **56**, 1634 (1968).
[30]A. S. Barker, Jr. and A. J. Sievers, Rev. Mod. Phys. **47**, S1 (1975).
[31]I. F. Chang and S. S. Mitra, Adv. Phys. **20**, 359 (1971).
[32]L. Genzel, T. P. Martin, and C. H. Perry, Phys. Status Solidi B **62**, 83 (1974).
[33]O. K. Kim and W. G. Spitzer, J. Appl. Phys. **50**, 4362 (1979).
[34]B. Jusserand and J. Sapriel, Phys. Rev. B **24**, 7194 (1981).
[35]M. Ilegems and G. L. Pearson, Phys. Rev. B **1**, 1576 (1970).
[36]I. F. Chang and S. S. Mitra, Phys. Rev. **172**, 924 (1968); Phys. Rev. B **2**, 1215 (1970).
[37]H. Harada and S. Narita, J. Phys. Soc. Jpn. **30**, 1628 (1971).
[38]R. Bonneville, Phys. Rev. B **24**, 1987 (1981).
[39]C. W. Myles, Phys. Rev. B **28**, 4519 (1983), and references therein.
[40]R. Bonneville, Phys. Rev. B **29**, 907 (1984).
[41]M. G. Holland, in *Semiconductors and Semimetals*, edited by R. K. Willardson and A. C. Beer (Academic, New York, 1967), Vol. 2, p. 3.
[42]Y. S. Touloukian, R. K. Kirby, R. E. Taylor, and T. Y. R. Lee, Thermophys. Prop. Matter **13**, 747 (1977).
[43]U. Piesbergen, in *Semiconductors and Semimetals*, edited by R. K. Willardson and A. C. Beer (Academic, New York, 1967), Vol. 2, p. 49.
[44]P. M. Marcus and A. J. Kennedy, Phys. Rev. **144**, 459 (1959).
[45]E. F. Steigmeier, Appl. Phys. Lett. **3**, 6 (1963).
[46]P. D. Maycock, Solid-State Electron. **10**, 161 (1967).
[47]B. Abeles, Phys. Rev. **131**, 1906 (1963).
[48]W. Both and F. P. Herrmann, Cryst. Research Technol. **17**, K117 (1982).
[49]M. A. Afromowitz, J. Appl. Phys. **44**, 1292 (1973).
[50]W. B. Joyce and R. W. Dixon, J. Appl. Phys. **46**, 855 (1975).
[51]D. J. Stukel and R. N. Euwema, Phys. Rev. **188**, 1193 (1969).
[52]A. Onton, in *Proceedings of the 10th International Conference on the Physics of Semiconductors* (Cambridge, Mass., 1970), p. 107.
[53]W. H. Berninger and R. H. Rediker, Bull. Am. Phys. Soc. **16**, 305 (1971).
[54]O. Berolo and J. C. Woolley, Can. J. Phys. **49**, 1335 (1971).
[55]E. Hess, I. Topol, K.-R. Schulze, H. Neumann, and K. Unger, Phys. Status Solidi B **55**, 187 (1973).
[56]R. L. Sarkar and S. Chatterjee, Phys. Status Solidi B **94**, 641 (1979).
[57]H. J. Lee, L. Y. Juravel, and J. C. Woolley, Phys. Rev. B **21**, 659 (1980).
[58]A.-B. Chen and A. Sher, Phys. Rev. B **22**, 3886 (1980).
[59]G. B. Stringfellow, J. Electron. Mater. **10**, 919 (1981).
[60]A.-B. Chen and A. Sher, Phys. Rev. B **23**, 5360 (1981).
[61]H. C. Casey, Jr. and M. B. Panish, *Heterostructure Lasers* (Academic, New York, 1978), Parts A and B.
[62]W. D. Laidig, D. K. Blanks, and J. F. Schetzina, J. Appl. Phys. **56**, 1791 (1984).
[63]M. Erman, J. B. Theeten, P. Frijilink, S. Gaillard, F. J. Hia, and C. Alibert, J. Appl. Phys. **56**, 3421 (1984).
[64]M. Cardona, K. L. Shaklee, and F. H. Pollak, Phys. Rev. **154**, 696 (1967).
[65]P. Parayanthal, C. S. Ro, F. H. Pollak, C. R. Stanley, G. W. Wicks, and L. F. Eastman, Appl. Phys. Lett. **43**, 109 (1983).
[66]R. Braunstein and E. O. Kane, J. Phys. Chem. Solids **23**, 1423 (1962).
[67]A. G. Milnes and D. L. Feucht, *Heterojunctions and Metal-Semiconductor Junctions* (Academic, New York, 1972).
[68]R. S. Bauer, P. Zurcher, and H. W. Sang, Jr., Appl. Phys. Lett. **43**, 663 (1983).
[69]W. E. Spicer and R. L. Bell, Pub. Astron. Soc. Pacific **84**, 110 (1972).
[70]R. Dingle, W. Wiegmann, and C. H. Henry, Phys. Rev. Lett. **33**, 827 (1974).
[71]R. L. Anderson, Solid-State Electron. **5**, 341 (1962).
[72]By an application of *C-V* profiling, Kroemer *et al.* [H. Kroemer, Wu-Yi Chien, J. S. Harris, Jr., and D. D. Edwall, Appl. Phys. Lett. **36**, 295 (1980)] have found the conduction-band discontinuity for an LPE grown $GaAs/Al_{0.3}Ga_{0.7}As$ heterojunction to be $\Delta E_c = 0.248$ eV, corresponding to about $0.66(E_{g2} - E_{g1})$ rather than Dingle's value $0.85(E_{g2} - E_{g1})$ [see Ref. 70]. They have speculated that the difference is attributed to composition grading during LPE growth.
[73]Recently, Watanabe *et al.* (M. O. Watanabe, J. Yoshida, M. Mashita, T. Nakanishi, and A. Hojo, in Ext. Abs. 16th Conf. on Solid State Devices and Materials, Kobe, 1984, p. 181) have also employed a *C-V* profiling technique to investigate the $GaAs/Al_xGa_{1-x}As$ heterojunction interface and obtained that $\Delta E_c = 0.62(E_{g2} - E_{g1})$ for the abrupt heterojunction.
[74]W. Paul, J. Appl. Phys. **32**, 2082 (1961).
[75]N. Lifshitz, A. Jayaraman, R. A. Logan, and R. G. Maines, Phys. Rev. B **20**, 2398 (1979).
[76]J. C. Phillips, *Bonds and Bands in Semiconductors* (Academic, New York, 1973).
[77]D. L. Camphausen, G. A. N. Connell, and W. Paul, Phys. Rev. Lett. **26**, 184 (1971).
[78]P. J. Dean and D. G. Thomas, Phys. Rev. **150**, 690 (1966).
[79]P. J. Dean, G. Kaminsky, and R. B. Zetterstrom, J. Appl. Phys. **38**, 3551 (1967).
[80]D. K. Kyser and V. Rehn, Phys. Rev. Lett. **40**, 1038 (1978).
[81]M. Zvara, Phys. Status Solidi **27**, K157 (1968).
[82]R. R. L. Zucca and Y. R. Shen, Phys. Rev. B **1**, 2668 (1970).
[83]B. Monemar, Phys. Rev. B **8**, 5711 (1973).
[84]The temperature variation of the band-gap energy can be expressed more rigorously by using the Varshni equation [Y. P. Varshni, Physica **34**, 149 (1967)]:

$$E_g^a(T,x) = E_g^a(0,x) - \alpha_g^a T^2/(T+\beta_g^a),$$

with coefficients α_g^a, β_g^a of Aspnes [D. E. Aspnes, Phys. Rev. B **14**, 5331 (1976)]:

$$\alpha_g^\Gamma = 5.41\times10^{-4}\ \text{eV/K}^2,$$
$$\alpha_g^X = 4.60\times10^{-4}\ \text{eV/K}^2,$$
$$\alpha_g^L = 6.05\times10^{-4}\ \text{eV/K}^2,$$
$$\beta_g^{\Gamma,X,L} = 204\ \text{K}.$$

[85]D. L. Rode, in *Semiconductors and Semimetals*, edited by R. K. Willardson and A. C. Beer (Academic, New York, 1975), Vol. 10, p. 1.
[86]O. Berolo, J. C. Woolley, and J. A. Van Vechten, Phys. Rev. B **8**, 3794 (1973).
[87]J. B. Restorff, B. Houston, J. R. Burke, and R. E. Hayes, Appl. Phys. Lett. **32**, 189 (1978).
[88]R. J. Nicholas, R. A. Stradling, and J. C. Ramage, J. Phys. C **12**, 1641 (1979).
[89]R. J. Nicholas, S. J. Sessions, and J. C. Porta, Appl. Phys. Lett. **37**, 178 (1980).
[90]E. H. Perea, E. Mendez, and C. G. Fonstad, J. Electron. Mater. **9**, 459 (1980).
[91]D. Olego, T. Y. Chang, E. Silberg, E. A. Caridi, and A. Pinczuk, Appl. Phys. Lett. **41**, 476 (1982).
[92]R. J. Nicholas, J. C. Portal, C. Houlbert, P. Perrier, and T. P. Pearsall, Appl. Phys. Lett. **34**, 429 (1979).
[93]M. Cardona and D. L. Greenaway, Phys. Rev. **125**, 1291 (1962).
[94]P. Lawaetz, Phys. Rev. B **4**, 3460 (1971).
[95]C. Hermann and T. P. Pearsall, Appl. Phys. Lett. **38**, 450 (1981).
[96]R. Dingle, R. A. Logan, and J. R. Arthur, Jr., in *Gallium Arsenide and Related Compounds* (Inst. of Phys., London, 1977), p. 210.
[97]K. Kaneko, M. Ayabe, and N. Watanabe, in *Gallium Arsenide and Related Compounds* (Inst. of Phys., London, 1977), p. 216.
[98]J. J. Yang, L. A. Moudy, and W. I. Simpson, Appl. Phys. Lett. **40**, 244 (1982).
[99]T. Ishikawa, J. Saito, S. Sasa, and S. Hiyamizu, Jpn. J. Appl. Phys. **21**, L675 (1982).
[100]T. Ishibashi, S. Tarucha, and H. Okamoto, Jpn. J. Appl. Phys. **21**, L476 (1982).
[101]N. Chand, T. Henderson, J. Klem, W. T. Masselink, R. Fischer, Y.-C. Chang, and H. Morkoç, Phys. Rev. B **30**, 4481 (1984).
[102]C. Mailhiot, Y.-C. Chang, and T. C. McGill, Phys. Rev. B **26**, 4449 (1982), and references therein.
[103]K. Tanaka, M. Nagaoka, and T. Yamabe, Phys. Rev. B **28**, 7068 (1983).
[104]C. Priester, G. Allan, and M. Lannoo, Phys. Rev. B **28**, 7194 (1983).
[105]W. T. Masselink, Y.-C. Chang, and H. Morkoç, Phys. Rev. B **28**, 7373 (1983).

[106]S. M. Sze, *Physics of Semiconductor Devices* (Wiley, New York, 1981).
[107]G. G. Kleiman and M. Fracastoro-Decker, Phys. Rev. B **21**, 3478 (1980).
[108]K. Masu, M. Konagai, and K. Takahashi, J. Appl. Phys. **51**, 1060 (1980).
[109]J. C. M. Henning, J. J. P. Noijen, and A. G. M. de Nijs, Phys. Rev. B **27**, 7451 (1983).
[110]G. E. Pikus and G. L. Bir, Sov. Phys.-Solid State **1**, 136 (1959).
[111]M. Cardona, *Light Scattering in Solids* (Springer, Berlin, 1975), Vol. 1, p. 1.
[112]P. Lawaetz, Phys. Rev. **166**, 763 (1968); **174**, 867 (1968); **183**, 730 (1969).
[113]J. D. Wiley, Solid State Commun. **8**, 1865 (1970).
[114]A. Gavini and M. Cardona, Phys. Rev. **177**, 1351 (1969); B **1**, 672 (1970).
[115]J. D. Wiley and M. DiDomenico, Jr., Phys. Rev. B **2**, 427 (1970).
[116]See, for example, G. L. Bir and G. E. Pikus, *Symmetry and Strain-Induced Effects in Semiconductors* (Wiley, New York, 1974).
[117]H. Kressel and J. K. Butler, *Semiconductor Lasers and Heterojunction LEDs* (Academic, New York, 1977).
[118]G. H. Olsen and M. E. Ettenberg, in *Crystal Growth: Theory and Techniques*, edited by C. H. L. Goodman (Plenum, New York, 1978), Vol. 2, p. 1.
[119]F. K. Reinhart and R. A. Logan, J. Appl. Phys. **44**, 3171 (1973).
[120]K. Röll, J. Appl. Phys. **47**, 3224 (1976).
[121]S. Kishino, N. Chinone, H. Nakashima, and R. Ito, Appl. Phys. Lett. **29**, 488 (1976).
[122]G. H. Olsen and M. Ettenberg, J. Appl. Phys. **48**, 2543 (1977).
[123]G. A. Rozgonyi, P. M. Petroff, and M. B. Panish, J. Crystal Growth **27**, 106 (1974).
[124]J. P. van der Ziel and A. C. Gossard, J. Appl. Phys. **48**, 3018 (1977).
[125]W. Pötz and P. Vogl, Phys. Rev. B **24**, 2025 (1981).
[126]R. L. Schmit and M. Cardona, in *Proceedings of the International Conference on the Physics of Semiconductors* (Marves, Rome, 1976), p. 239.
[127]R. L. Schmidt, B. D. McCombe, and M. Cardona, Phys. Rev. B **11**, 746 (1975).
[128]M. H. Grimsditch, D. Olego, and M. Cardona, Phys. Rev. B **20**, 1758 (1979).
[129]W. A. Harrison, Phys. Rev. **104**, 1281 (1956).
[130]E. M. Conwell, *High Field Transport in Semiconductors* (Academic, New York, 1967).
[131]The value dE_{ca}/dP could be given by the equation: $dE_{ca}/dP - dI/dP$, where I is the energy of the top of the valence band at $\mathbf{k} = 0$.
[132]A. K. Saxena and K. S. Gurumurthy, J. Phys. Chem. Solids **43**, 801 (1982).
[133]G. A. Samara, Phys. Rev. B **27**, 3494 (1983), and references therein.
[134]R. E. Fern and A. Onton, J. Appl. Phys. **42**, 3499 (1971).
[135]S. Hudgens, M. Kastner, and H. Fritzsche, Phys. Rev. Lett. **33**, 1552 (1974).
[136]T. Sahu and P. K. Misra, Phys. Rev. B **26**, 6795 (1982).
[137]S. H. Wemple and M. DiDomenico, Jr., Phys. Rev. B **3**, 1338 (1971).
[138]G. Arlt and P. Quadflieg, Phys. Status Solidi **25**, 323 (1968).
[139]J. C. Phillips and J. A. Van Vechten, Phys. Rev. Lett. **23**, 1115 (1969).
[140]H. Hübner, Phys. Status Solidi B **57**, 627 (1973).
[141]M. Miura, H. Murata, Y. Shino, and K. Iishi, J. Phys. Chem. Solids **42**, 931 (1981).
[142]J. B. McKitterick, Phys. Rev. B **28**, 7384 (1983).
[143]D. Berlincourt, H. Jaffe, and L. R. Shiozawa, Phys. Rev. **129**, 1009 (1963).
[144]N. I. Meyer and M. H. Jørgensen, in *Advances in Solid State Physics*, edited by O. Madelung (Pergamon, Vieweg, 1970), p. 21.
[145]D. L. Spears, Phys. Rev. B **2**, 1931 (1970).
[146]P. O. Sliva and R. Bray, Phys. Rev. Lett. **14**, 372 (1965).
[147]J. T. Devreese, *Polarons in Ionic Crystals and Polar Semiconductors* (North-Holland, Amsterdam, 1972).
[148]S. D. Sarma, Phys. Rev. B **27**, 2590 (1983), and references therein.
[149]D. C. Langreth, Phys. Rev. **159**, 717 (1967).
[150]A. K. Saxena, Phys. Rev. B **24**, 3295 (1981).
[151]G. Hill and P. N. Robson, J. Phys. 42 (suppl.), C7-335 (1981).
[152]P. Banerjee, P. K. Bhattacharya, M. J. Ludowise, and W. T. Dietze, IEEE Electron Dev. Lett. **EDL-4**, 283 (1983).
[153]P. K. Bhattacharya, U. Das, and M. J. Ludowise, Phys. Rev. B **29**, 6623 (1984).
[154]Y. Takeda, M. A. Littlejohn, and R. J. Trew, Appl. Phys. Lett. **40**, 836 (1982).
[155]T. Sugeta, A. Majerfeld, A. K. Saxena, and P. N. Robson, Appl. Phys. Lett. **31**, 842 (1977).
[156]C. L. Collins and P. Y. Yu, Phys. Rev. B **30**, 4501 (1984).
[157]W. Fawcett, A. D. Boardman, and S. Swain, J. Phys. Chem. Solids **31**, 1963 (1970).
[158]J. G. Ruch and G. S. Kino, Appl. Phys. Lett. **10**, 40 (1967).
[159]D. K. Ferry, Phys. Rev. B **12**, 2361 (1975).
[160]M. A. Littlejohn, J. R. Hauser, T. H. Glisson, D. K. Ferry, and J. W. Harrison, Solid-State Electron. **21**, 107 (1978).
[161]D. L. Rode and P. A. Fedders, J. Appl. Phys. **54**, 6425 (1983), and references therein.
[162]P. A. Fedders and C.W. Myles, Phys. Rev. B **29**, 802 (1984).
[163]C. A. Coulson, L. B. Redei, and D. Stocker, Proc. R. Soc. London **270**, 357 (1962).
[164]R. S. Knox, *Theory of Excitons* (Academic, New York, 1963).
[165]J. O. Dimmock, in *Semiconductors and Semimetals*, edited by R. K. Willardson and A. C. Beer (Academic, New York, 1967), Vol. 3, p. 259.
[166]M. A. Gilleo, P. T. Bailey, and D. E. Hill, Phys. Rev. **174**, 898 (1968).
[167]D. Henning and R. Strehlow, Phys. Status Solidi B **107**, 283 (1981).
[168]E. F. Schubert, E. O. Göbel, Y. Horikoshi, K. Ploog, and H. J. Queisser, Phys. Rev. B **30**, 813 (1984).
[169]H. C. Casey, Jr., D. D. Sell, and M.B. Panish, Appl. Phys. Lett. **24**, 63 (1974).
[170]H. Burkhard, J. Appl. Phys. **55**, 503 (1984); B. Broberg and S. Lindgren, J. Appl. Phys. **55**, 3376 (1984).
[171]P. A. Kirkby, P. R. Selway, and L. D. Westbrook, J. Appl. Phys. **50**, 4567 (1979).
[172]C. W. Higginbotham, M. Cardona, and F. H. Pollak, Phys. Rev. **184**, 821 (1969).
[173]J. A.Van Vechten, Phys. Rev. **182**, 891 (1969).
[174]P. Y. Yu, M. Cardona, and F. H. Pollak, Phys. Rev. B **3**, 340 (1971).